FULL PAPER

Cyclodextrin-based organic radical contrast agents for *in vivo* imaging of glioma

Lucio Melone*[a,b], Alice Bach[c], Gianrico Lamura[d], Fabio Canepa[d,e] Riikka Nivajärvi[f], Venla Olsson[g] and Mikko Kettunen*[f]

[a] Prof. L. Melone
Department of Chemistry, Materials and Chemical Engineering "G. Natta"
Politecnico di Milano
Via Mancinelli 7, 20131, Milano (Italy)
E-mail: lucio.melone@polimi.it
[b] Prof. L., Melone
UniversitàTelematica e-Campus
Via Isimbardi 10, 22060, Novedrate, Como (Italy)
[c] Dr. A. Bach,
Polytech Sorbonne, 4 place Jussieu, 75252 Paris Cedex 05, France
[d] Dr. G. Lamura, Prof. F. Canepa
CNR-SPIN
Corso Perrone 24, 16152, Genoa (Italy)
[e] Prof. F. Canepa
Department of Chemistry and Industrial Chemistry
Università di Genova
Via Dodecaneso, 31, 16146 Genova (Italy)
[f] Ms. R. Nivajärvi, Dr. M. Kettunen
Kuopio Biomedical Imaging Unit, A.I. Virtanen Institute for Molecular Sciences
University of Eastern Finland
Neulaniementie 2, 70211 Kuopio (Finland)
E-mail: mikko.kettunen@uef.fi
[g] Ms. V. Olsson
Molecular Medicine, A.I. Virtanen Institute for Molecular Sciences
University of Eastern Finland
Neulaniementie 2, 70211 Kuopio (Finland)

Supporting information for this article is given via a link at the end of the document.

Abstract: Cyclodextrins (CDs), a family of cyclic oligosaccharides with n=6, 7 or 8 anhydroglucose units, are suitable for the preparation of supramolecular organic radical contrast agents (ORCAs). In this paper we consider different aspects of the CDs functionalization with (2,2,6,6-tetramethylpiperidin-1-yl)oxyl (TEMPO) radicals with the aim to create a water soluble family of compounds for the *in vivo* detection of glioma tumor in animal models. A first set of CD-based polynitroxides (**CDn1**, n=6,7,8 indicates the number of both TEMPO and anhydroglucose units) was investigated by Superconducting Quantum Interference Devices (SQUID) magnetometry in order to define the role of the CD macrocycle on the effective magnetic moment (μ_{eff}). It was found that μ_{eff} increased from 3.892 μ_B(**CD61**) to 4.522 μ_B (**CD81**). Intra-molecular antiferromagnetic (AF) interactions limited the upper bound for μ_{eff} when the number of TEMPO radical per molecule increased from n=6 to n=8. By a functionalization sequence based on thiol-ene and copper(I)-catalyzed alkyne-azide "click reactions", a set of water soluble CD-based ORCAs was prepared (**CDn8**, n=6, 7, 8). Their ^{1}H water relativities r_1 were comprised between 0.739 mM^{-1} s^{-1} (**CD68**) to 1.047 mM^{-1} s^{-1} (**CD88**) in D_2O/H_2O 9:1 (v:v) solvent at 300 K. One of such compounds (**CD78**) was tested on glioma-bearing rats and compared with gadolinium-diethylenetriamine pentaacetic acid (Gd-DTPA). **CD78** was characterized by reduced side effects and good relaxivity *in vivo*.

Introduction

Magnetic Resonance Imaging (MRI) is a non-invasive imaging technique widely adopted in the clinical practice for diagnostic purposes.[1] Compared to other imaging techniques that rely on ionizing radiations such as positron emission tomography (PET) and computed tomography (CT), MRI is based on the use of strong magnetic fields and it is considered relatively safe. Contrast Agents (CAs) are injected into the body of the patients before the scanning process in order to improve the MRI sensitivity. CAs cause a reduction of the relaxation times (longitudinal relaxation time, T_1, or transverse relaxation time, T_2) of surrounding water molecules in tissues. The magnitude of reduction of T_1 or T_2 depends on both the concentration of CA accumulated into the tissue and the tissue itself. The result is a significant improvement of contrast in the final images that facilitates the diagnosis of several pathologies including cancer.
Due to their excellent relaxation properties provided by the presence of seven unpaired electrons, Gd(III) ions are the heart of the majority of CAs on the market at the moment.[2] While inorganic Gd(III) salts are highly toxic, a large number of Gd-based CAs have been synthesized and marketed by chelating Gd(III) ions with suitable organic ligands in order to reduce the toxic effects.[2,3] While commercial Gd(III)-based CAs are designed to warrant a good stability of the complex from the administration to the final excretion from the body, and are well tolerated by many people over short time scales, toxicity issues have been reported in literature for patients suffering of renal insufficiency. Indeed, the administration of Gd(III) chelates seems

to be a triggering factor for the development of nephrogenic systemic fibrosis (NFS) thus Gd(III)-based CAs cannot be used for such kind of patients.[4]

In order to overcome such toxicity issues, organic radical contrast agents (ORCAs) based on nitroxides have been proposed as a possible alternative to Gd(III)-based CAs.[5, 40 41] If from one side nitroxides are relatively nontoxic, on the other side they undergo problems of different nature. Indeed, nitroxyl radicals have both the tendency to be reduced easily to the corresponding diamagnetic hydroxylamines after injection into the bloodstream and to provide low ^{1}H water relaxivities. The former issue can be overcome by the adoption of radicals with higher sterical hindrance.[6, 7] Furthermore, the sensitivity of nitroxyl radicals to the redox environment in tissues and organs has been fruitfully considered for magnetic resonance imaging purposes in several papers.[8-11] Higher ^{1}H water relaxivities can be obtained by increasing the spin density through the introduction of multiple radical centers on the same supramolecular structure. Relevant examples of polynitroxides for MRI have been provided in several studies.[5, 12-21]

Cyclodextrins (CDs), a class of macrocyclic oligosaccharides composed by 6, 7, or 8 glucosidic units (α-, β-, and γ-CD respectively), could be a valuable starting point for the synthesis of supramolecular ORCAs. CDs exhibit a three-dimensional structure with a truncated cone shape. The inner cavity of the cone has a hydrophobic character and can be involved in formation of host-guest complexes with several molecules.[22] The hydroxyl groups of each anydroglucose unit can be found on both the large rim (OH in position 2 and 3) and the small rim of the truncated cone (OH in position 6). They have different reactivity, thus several strategies for their selective functionalization have been proposed over the years.[23] Interesting examples of CD-based CAs, but still containing Gd(III) units, have been recently reported in literature putting well in evidence the high versatility of CDs for the creation of supramolecular CAs with high spin density, in particular through the formation of polyrotaxanes.[24-26]

The functionalization of β-CD by the introduction of one or seven (2,2,6,6-tetramethylpiperidin-1-yl)oxyl (TEMPO) radical moieties was proposed as potential supramolecular vectors for magnetic resonance imaging and investigated in terms of magnetic properties and ^{1}H water relaxivities.[27] Moreover, the use of CD functionalized with a single TEMPO unit has found application as doping agent for proton and carbon-13 dynamic nuclear polarization studies of natural and modified CDs.[28-30] The introduction of seven radical units on the small rim of the β-CD cone (compound **CD71** in Figure 1) allowed to increase the magnetic moment ($\mu_{eff}/\mu_B \approx 4.2$) and ^{1}H water relaxivity ($r_1 = 1.596$ mM^{-1} s^{-1}) compared to the analogous derivative with a single TEMPO unit ($\mu_{eff}/\mu_B \approx 1.7$ and $r_1 = 0.323$ mM^{-1} s^{-1}). Unfortunately, this compound was not suitable for the direct application as *in vivo* CA, due to its low solubility in water. Therefore, in the present work, we propose a synthetic approach that leads to the preparation of water-soluble CD polynitroxides on gram scale and their use for *in vivo* MRI studies. In particular, the following aspects are covered in this paper: i) a detailed investigation by SQUID magnetometry of the role of the CD cavity (α-, β-, and γ-CD) on the magnetic properties of three CDs functionalized with TEMPO radical moieties (compounds **CDn1** in Figure 1, n=6, 7, 8); ii) the synthesis of different new CD polynitroxides by a suitable sequence of thiol-ene and copper(I)-catalyzed alkyne-azide "click reactions" (see Figure 1); iii) the application of a selected water-soluble derivative (**CD78** in Figure 1) for the *in vivo* imaging of glioma.

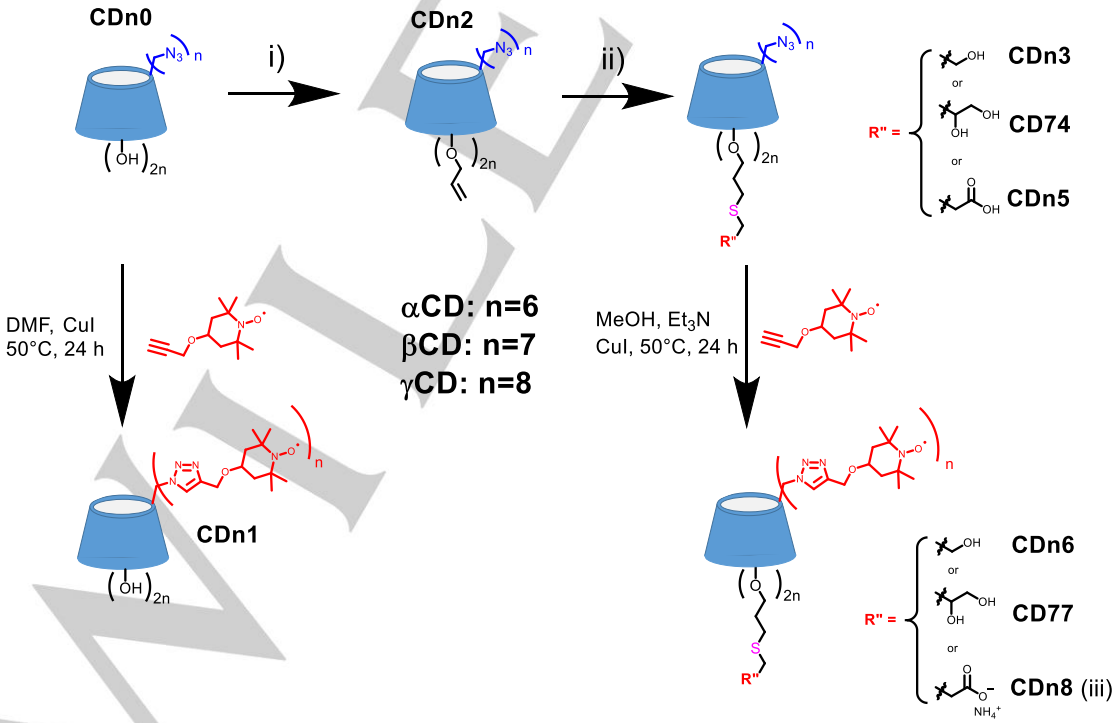

Figure 1. Synthetic scheme. i) anhydrous DMF, NaH, allylbromide, 0°C, 24h; ii) MeOH, benzophenone, 2-mercaptoethanol (**CDn3**), or 1-thioglycerol (**CDn4**), or 3-mercaptopropionic acid (**CDn5**), UV-light (365nm), 25°C, 24h; iii) MeONa was added to the solution of **CDn5** in MeOH before the addition of Et_3N. The final derivative was obtained by precipitation in HCl (aq, 1M) at 0°C, followed by solubilization with NH_4OH(aq) and freeze-drying.

Results and Discussion

The ^{1}H water relaxivities r_1 (longitudinal) and r_2 (transversal) of any CA depend quadratically by its effective magnetic moment μ_{eff}.[31] Anyway, r_1 and r_2 can be affected by temperature, field strength, and substance in which the contrast agent is dissolved. On the contrary, μ_{eff} is a strictly related to the CA chemical structure. For this reason, in order to evaluate the role played by the CD macrocycle and the number of radicals units, the measurement of μ_{eff} for the derivatives **CDn1** (n=6,7,8) was carried out by DC-SQUID magnetometry. Such compounds are not soluble in water and hence do not represent our final target However, in our molecular design process, they can be a suitable molecular model for investigating the relations underlying between chemical structure and magnetic properties.

The temperature dependence of the inverse molar magnetic susceptibility $1/\chi_m$ measured by applying a magnetic field of 50 mT for the samples **CDn1** (n=6, 7, 8) is shown in the top panel of Figure 2. We notice the following: (a) all the samples show a linear temperature behavior as expected in the case of non-interacting paramagnetic moments. The resulting fitting parameter are reported in Table 1. (b) The slope increases with increasing number of TEMPO units per molecule. Since the effective magnetic moment carried per molecule μ_{eff} is inversely proportional to the square root of the Curie constant, this indicates an increase of μ_{eff} from 3.98 up to 4.52 in units of Bohr magneton (μ_B). (c) The Curie-Weiss temperature is negative for all the samples indicating the presence of weak antiferromagnetic (AF) interactions both of inter- and intra-molecular origin. In the bottom panel of Figure 2 $\chi_m T$ as a function of temperature is presented. $\chi_m T$ is almost temperature independent down to 30 K, below which temperature a downward curvature indicates the presence of AF interactions.

Table 1. Molar Curie-Weiss constant C_m, Curie-Weiss temperature Θ, effective magnetic moments μ_{eff} and saturated magnetization M_S for samples **CDn1**, n=6, 7, 8.

Sample	Curie-Weiss temperature Θ [a]	Curie-Weiss constant C_m [a]	μ_{eff} [b]	M_S [c]
	[K]	[×10^{-5} m^3 K mol^{-1}]	[μ_B]	[μ_B]
CD61	-1.48 (6)	2.493 (1)	3.982 (1)	5.40 (3)
CD71	-1.5 (2)	2.856 (3)	4.262 (1)	6.39 (3)
CD81	-0.6 (2)	3.215 (4)	4.522 (1)	7.30 (3)

[a] C_m and Θ resulted from the linear fits on the inverse magnetic susceptibility represented in the top panel of figure i.1 for samples **CD61**, **CD71** and **CD81**.
[b] The effective magnetic moment μ_{eff} per molecule was extracted from the Curie constant $C_n = \mu_0 N_A \mu_{eff}^2 \mu_B^2 / 3k_B$, where N_A is the Avogadro's number, k_B is the Boltzmann constant, μ_0 is the vacuum magnetic permeability and μ_B is the Bohr magneton constant.
[c] Obtained by a linear fit of the magnetic moment per molecule versus $(\mu_0 H/T)^{-1}$ in the high field regime (see text for details).

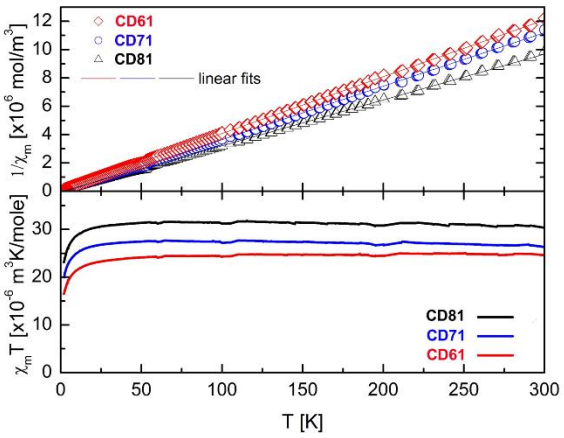

Figure 2. $1/\chi_m$ (top panel) and $\chi_m \cdot T$ (bottom panel) as a function of temperature for **CD61**, **CD71** and **CD81**, respectively. The continuous line represents the linear fits (see text for details).

In Figure 3 the isothermal magnetization expressed in unit of μ_B per molecule as a function of H/T at 2, 5 and 10 K is shown. We can notice some interesting features: (i) the experimental points do not collapse on the same line as required for a system of non-interacting magnetic moments. This is true for all the tested samples. (ii) A simple Brillouin model fit (not shown for sake of clarity) fails to take into account the experimental data contrary to the case of mono-TEMPO radical magnetic moment.[27] Both issues (i) and (ii) likely suggest that by increasing the number of TEMPO radical per molecule both the inter- and the intra-molecular AF exchange interactions increase. In particular, enhanced intra-molecular AF interaction could strongly limit the upper bound for μ_{eff} when the number of TEMPO radical per molecule is increased. In order to estimate the saturation magnetic moment carried per molecule M_S we study the low temperature data by using the Langevin model function in the high field limit. In such case, the magnetic moment per molecule expressed in Borh magneton units scales linearly with 1/H as $M_S - \alpha(T/\mu_0 H)$, α being a scaling constant. In Figure 4 we plot the magnetic moment measured at 2K as a function of $(\mu_0 H/T)^{-1}$ with the respective linear fit limited to the high field interval ($3.5T \leq \mu_0 H \leq 5.5T$). The intercept at the limit $(\mu_0 H/T)^{-1} \rightarrow 0$ gives an estimation of M_S. These data have been summarized in Table 1. It is worth noting that at high field and low temperature M_S approaches reasonably the values expected for a system of n independent magnetic moments per molecule.

In order to obtain a water soluble compound suitable for the *in vivo* injection, we decided to postpone the introduction of the TEMPO moieties by following the route described in Figure 1. Starting from the azido derivatives **CDn0**, n=6, 7, 8, the wider rim of the CD cavity was first functionalized by introducing allyl moieties (**CDn2**, n=6, 7, 8). The obtained compounds were further modified by a thiol-ene reaction with a thiol-containing molecule.[32] Initially we used 2-mercaptoethanol with the hope that the introduction of arms ending with primary –OH groups could be enough to make the final product soluble in water. The derivatives **CDn3** (n=6,7,8) were thus obtained in a smooth way and in high yield.

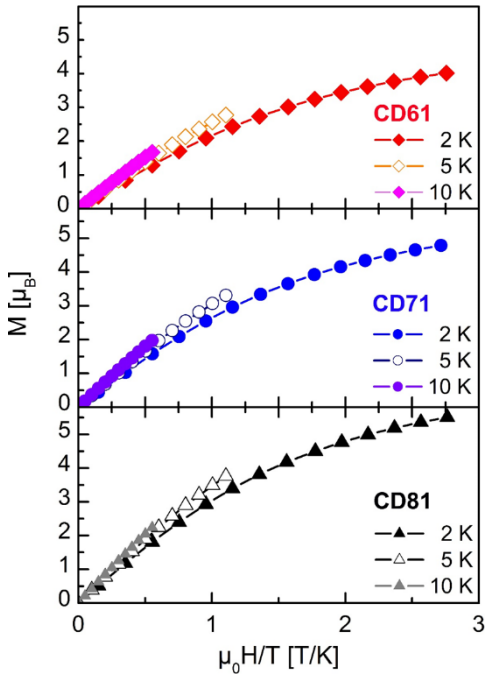

Figure 3. Isothermal magnetization measurements as a function of H/T at T=2, 5, 10 K for **CD61** (top panel), **CD71** (middle panel) and **CD81** (bottom panel) samples, respectively.

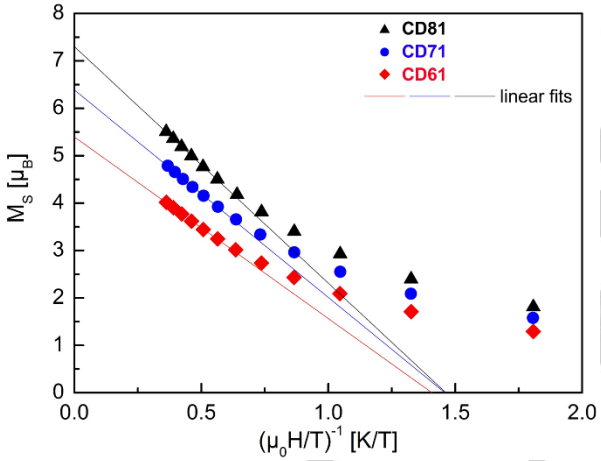

Figure 4. Magnetic moment per molecule M versus $(\mu_0 H/T)^{-1}$ taken at 2 K. The continuous lines represent linear fits limited to the high field interval ($3.5T \leq \mu_0 H \leq 5.5T$). The intercept at the limit $(\mu_0 H/T)^{-1} \rightarrow 0$ gives an estimation of the saturated magnetic moment per molecule M_S.

Finally, the click reaction with 4-(propargyloxy)-TEMPO afforded the products **CDn4** (n=6,7,8). Unfortunately, all **CDn4** compounds were scarcely soluble in water but the simplicity of the protocol and the good yields of the final products induced us to keep this procedure and to test a different thiol-containing molecule. Using 1-thioglycerol the compound **CD74** was synthesized (in this case the synthesis was limited to the β-CD derivative). **CD74** was finally converted to **CD77**. As **CDn4**, also **CD77** did not show remarkable solubility in water despite the presence of arms ending with glycerol moieties. Therefore, we recognized the need of preparing a compound with a clearer amphiphilic character by introducing, on the CD wider rim, moieties with a stronger polar behavior able to counterbalance the lipophilicity of the TEMPO moieties on the narrower rim. For this reason, the compound 3-mercaptopropionic acid was reacted under the same protocol with **CDn2** (n=6,7,8) affording the derivatives **CDn5** (n=6,7,8). The click reaction of **CDn5** with 4-(propargyloxy)-TEMPO was carried out under conditions similar to those considered for the preparation of the other compounds with few modifications. Indeed, **CDn5** was first converted to the corresponding sodium salt by the addition of a slight excess of sodium methoxide. This avoided the formation of a salt between **CDn5** and Et_3N added as co-catalyst for the click reaction. After removing the copper salts by filtration on silica gel and recovering the excess (propargyloxy)-TEMPO, the final products **CDn8** (n=6,7,8) were obtained as ammonium salts by a two-steps purification procedure. In the first step **CDn8** (n=6,7,8) was obtained as solid precipitate in a HCl aqueous solution (pH 2) at 0°C. In the second step **CDn8** (n=6,7,8) was converted to the corresponding ammonium salt by the addition of an excess of NH_4OH(aq) and obtained as reddish solid by freeze-drying. The use of aqueous media in the last part of this purification protocol minimizes the risk of contamination with traces of organic solvents and is more suitable in view of the final *in vivo* application.

All **CDn8** (n=6,7,8) can be easily dissolved in water. Figure 5 shows a 200 mM **CD78** aqueous solution. The maximum solubility was not determined. However, aqueous solutions more concentrated than 200 mM can be prepared despite they have the tendency to become qualitatively more viscous by increasing the amount of dissolved compound.

The ^{1}H water r_1 relaxivities were measured for all the synthesized compounds and the corresponding data are reported in Table 2. The water soluble compounds **CDn8** (n=6, 7, 8) were dissolved in D_2O/H_2O 9:1 (v:v) (entries 8-10). The remaining water insoluble compounds were dissolved in DMSO-d_6/H_2O 9:1 (entries 1-7). For comparison, the ^{1}H water r_1 relaxivities associated to commercial 4-hydroxy-TEMPO (TEMPOL) in both solvents were also measured (entries 11-12). The original data are reported in the Supplementary Information file (Fig.S28 – Fig.S30). With regard to compounds **CDn1**, n=6, 7, 8, r_1 values increase with n and follow the expected quadratic relation with μ_{eff} (Fig.S31). The same trend, with comparable values, was found with the compounds **CDn6** (n=6, 7, 8) and **CD77** confirming that the functionalization of the CD wider rim does not have remarkable effects on the radical units attached on the opposite side of the CD cavity. Unfortunately, the compounds **CDn8** (n=6, 7, 8) are not well soluble in DMSO-d_6/H_2O 9:1 for that a direct comparison with the other compounds cannot be done. This aspect becomes relevant if we consider that the r_1 values of such compounds are lower in D_2O/H_2O 9:1 (v:v) (the increase with n can be observed similarly to other compounds). However, as evidenced by the entries 11 and 12, the r_1 value associated to TEMPOL is also significantly reduced when D_2O/H_2O 9:1 (v:v) is used in place of DMSO-d_6/H_2O 9:1 (-43%). A similar percentage can be found, for example, between **CD78** (entry 9) and **CD71** (entry 2) (-42%) or between **CD88** (entry 10) and **CD81** (entry 3) (-42%). Such data show the relevant role played by the solvent in affecting the r_1 values.

Due to the importance of MRI as diagnostic technique for the visualization and quantification of tumors, we decided to test one our water soluble polynitroxides on glioma-bearing rats. Glioma is

indeed one of the most common and aggressive brain tumors with a grim prognosis.

Figure 5. CD78 aqueous solution (200 mM).

Less than 10% of patients survive more than five years with an average survival below 2 years.[33] Only **CD78** was selected for the *in vivo* application in order to limit the number of animal experiments and because its relaxivity value is intermediate to those of **CD68** and **CD88**. Moreover, **CD78** is prepared from β-CD that is the cheapest among all CDs. As comparison, the commercial gadolinium-diethylenetriamine pentaacetic acid (Gd-DTPA) was used in parallel experiments.

Upon injection of **CD78** into glioma-bearing rats, a decrease in tumor T_1 was observed (-0.23 ± 0.14 s measured 12 mins after the start of injection, p~0.00024, n=10) (Figure 6.a), whereas there was no change in brain T_1 (-0.01 ± 0.04 s). This resulted to a decreased tumor/tissue contrast due to their relaxation times being nearly same post-injection. However, analysis based on a pre/post difference image can be easily used in this tumor. No change in T_2 was observed. T_1 had returned to its original value by 55 minutes post-injection. For comparison, injection of Gd-DTPA led to a larger decrease in tumor T_1 (-1.08 ± 0.24 s, p~1.9*10^{-6}, n=8) that had not yet reached baseline by 1h after injection. In contrast to the other two contrast agents, TEMPOL did not show any decrease in tumor T_1 at 12 mins, and the kinetic analysis of the first 10 minutes showed that MRI signal returned to baseline within about 4 mins after TEMPOL injection (Supplementary Figure S33). This most likely reflects its rapid bio-reduction, although we cannot rule out that its smaller molecular size could also lead to a more rapid removal of the molecule. While both TEMPOL and **CD78** showed similar reduction rates *in vitro* (Figure S34), the in vivo results confirm an improved retention of the altered MR contrast with **CD78**.

When the relaxation data were converted to apparent tissue concentrations based on their relaxivities (0.71 $s^{-1}mM^{-1}$ and 4 $s^{-1}mM^{-1}$ for **CD78** and Gd-DTPA, respectively), the tumor concentrations at 12 mins were 0.08 ± 0.05 mM (p~0.00033, n=10) and 0.13 ± 0.07 mM (p~0.00051, n=8) for **CD78** and Gd-DTPA, respectively, and both showed an approximate dose response (Figure 6.c). Taking into account the variable dose used in the experiments, approximately 0.11 ± 0.06 %ID/g of **CD78** reached tumor (Figure 6.d). This was a third of Gd-DTPA reaching the tumor, 0.33 ± 0.11 %ID/g (difference between the two, p<~8*10^{-5}). The loss of contrast, estimated as exponential decay of over time, was significantly faster for **CD78** than for Gd-DTPA with half-lives of 17 ± 6 min and 39 ± 19 min, respectively (p~0.005). These two effects may reflect a combination of lower penetration and accelerated clearance of the **CD78** from tumor and loss of paramagnetism due to reduction of TEMPO moieties. While bulkier molecules tend to show enhanced accumulation to tumors due to their size (enhanced permeability and retention effect), at 5 kDA **CD78** may not access tumor tissue through the leaky blood vessels, and this effect may be amplified if the contrast agent forms assemblies. Kinetic analysis of the first 10 minutes showed much slower accumulation of **CD78** to the tumor tissue as evidenced by the slowly increasing signal (Figure S33). On the other hand, unlike TEMPOL, we do not expect **CD78** to penetrate the cells which may expose the CA to less reducing factors thereby slowing the loss of contrast. In one animal receiving **CD78**, the bladder was imaged 60 mins post-injection yielding 18 mM apparent **CD78** concentration (36% of injected dose) and a urine sample collected 90 mins post-injection had 30 mM (58% of injected dose). This suggest the majority of **CD78** is removed via kidneys. In the current study, the majority of the experiments used ~0.2 mmol kg^{-1}. This was selected based on the previously reported toxicity of TEMPO (up to 1.5 mmol kg^{-1}).[34] It is possible that higher doses of contrast agent could be used to improve the relaxation effect. In the current experiments the highest tested dose of **CD78** was 0.5 mmol kg^{-1}.

Table 2. *In vitro* ^{1}H water relaxivities (r_1) of the ORCAs proposed in this work (300 K, 9.4 T).[D]

Entry	Compound [C]	MW (g mol^{-1})	Solvent	r_1 (mM^{-1} s^{-1})
1	**CD61**	2384.68	A	1.288
2	**CD71**	2782.16	A	1.521
3	**CD81**	3179.62	A	1.796
4	**CD66**	3803.04	A	1.306
5	**CD76**	4436.88	A	1.435
6	**CD86**	5070.73	A	1.694
7	**CD77**	4857.24	A	1.480
8	**CD68**	4343.53	B	0.739
9	**CD78**	5067.45	B	0.877
10	**CD88**	5791.38	B	1.047
11	TEMPOL	172.25	A	0.298
12	TEMPOL		B	0.171

A: DMSO-d_6/H_2O 9:1 (v:v)

B: D_2O/H_2O 9:1 (v:v)

C: The relaxivity of Gd-DTPA is close to 4 mM^{-1} s^{-1}. See ref. 35 for further details.

D: r_1 values are related to the specific compounds and not to the single nitroxide units.

Conclusion

In summary, CDs (α-, β-, and γ-CD) can be easily functionalized with TEMPO radical moieties to provide a set of water soluble ORCAs (compounds **CDn8**, n=6, 7, 8). The protocol consists of: 1) the modification of the CD wider rim by the introduction of polar arms ending with carboxylic groups through a thiol-ene click reaction; 2) the introduction of TEMPO units on the CD smaller rim by copper(I)-catalyzed alkyne-azide “click reactions”. Such

compounds show good ^1H water r_1 relativities with values comprised between ~0.7 mM^{-1} s^{-1} and ~1.0 mM^{-1} s^{-1} in D_2O/H_2O 9:1 (v:v) solvent at 305K. As comparison, r_1 value for TE in the same solvent is significantly lower (~0.17 mM^{-1} s^{-1}) while r_1 for commercial Gd(DTPA) is close to 4 mM^{-1} s^{-1}.[35] Magnetic measurements carried out on a set of more primitive derivatives (**CDn1**, n=6, 7, 8) revealed that the effective magnetic moment (μ_{eff}) increases with the number of TEMPO units but its increase is strongly limited by antiferromagnetic (AF) spin-spin interactions.[42] This suggests that a future re-design of **CDn8** molecules, relatively to the side containing nitroxyl radicals, should be oriented towards a molecular structure with reduced AF interactions. This effort would warrant higher μ_{eff} and, therefore, higher relaxivities. The compound **CD78** was tested on glioma-bearing rats, and appeared to be tolerated by the animals at the tested dose. Tumor accumulation and retention of **CD78** resembled Gd(DTPA). After injection, **CD78** (~0.2 mmol kg^{-1}) provided a decrease of T_1, higher than TEMPOL (~1.6 mmol kg^{-1}), which did not show any detectable effect, but lower than Gd(DTPA) (~0.1 mmol kg^{-1}). Therefore, **CD78** had an improved *in vivo* bioavailability compared to TEMPOL but may still experience a loss of paramagnetism due to bioreduction of the TEMPO radicals. Perhaps this limitation could be overcome in a subsequent upgrade of the **CDn8** series by replacing TEMPO with radicals less sensitive to bioreduction like 2,2,6,6-tetraethylpiperidin-1-oxyl (TEEPO).[7, 36]

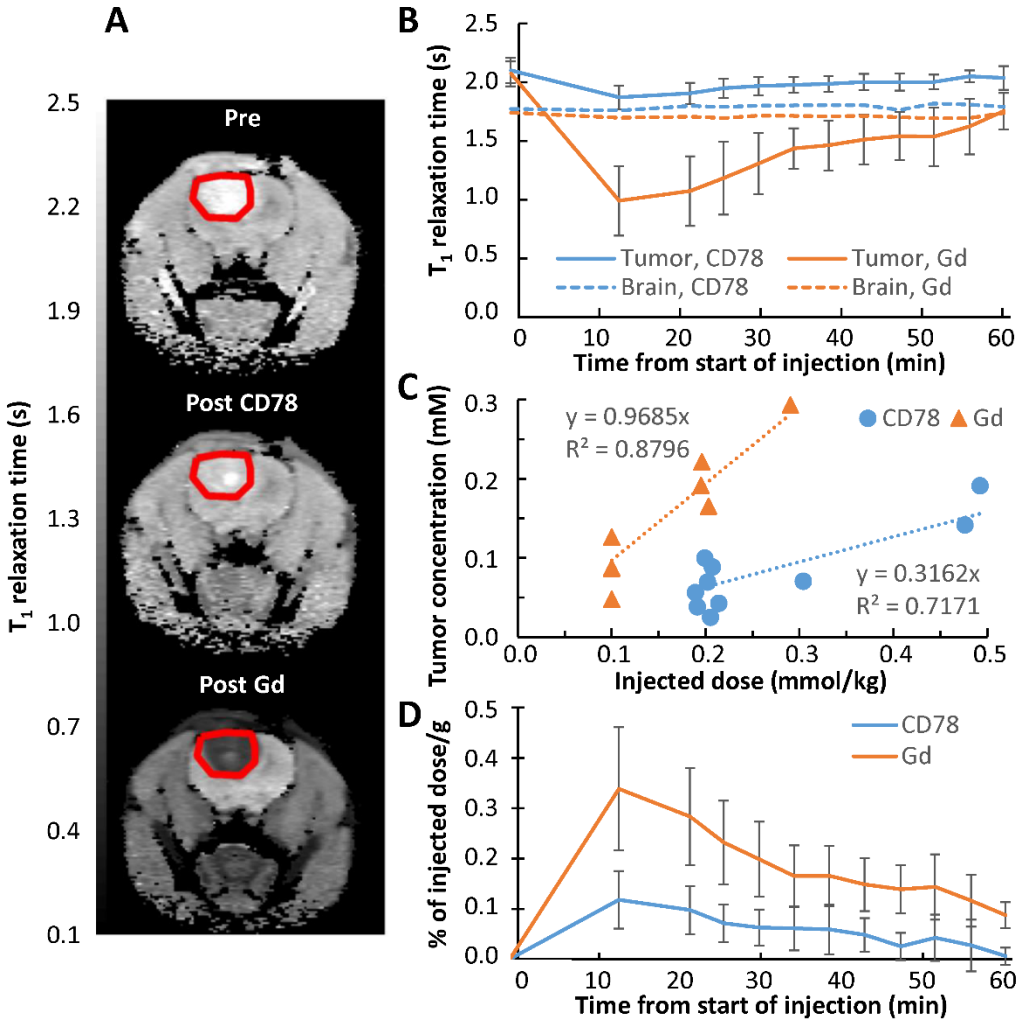

Figure 6. T_1 relaxation maps in a glioma-bearing rat (tumor marked with red line) before and after 0.2 mmol/kg injection of either nitroxyl or Gd-based contrast agent (A) and corresponding time courses in all studied animals (CD78, N = 10, Gd-DTPA, N = 8, the concentration varied from 0.2 to 0.5 mmol/kg for CD78 and from 0.1 to 0.3 mmol/kg for Gd-DTPA) (B). Both contrast agent lead to decreased T_1 with Gd causing a larger effect. A higher apparent tumor concentration was observed for both CA when injected dose was increased (C), but only a small fraction of both CA was present in tumor at 12 min post-injection (D). Values in B and D are given as mean + SD.

Experimental Section

General

Cyclodextrins (αCD, βCD, γCD) and other reagents and solvents were commercially available and used as received unless otherwise stated. Hexakis-6-iodo-6-deoxy-αCD, Heptakis-6-iodo-6-deoxy-βCD and Octakis-6-iodo-6-deoxy-γCD and the corresponding azides (**CDn0**, n=6, 7, 8) were synthesized according to literature.[38] 4-(propargyloxy)-TEMPO was prepared as reported by Bogdan and McQuade.[39] The derivatives **CDn1** (n=6, 7, 8) were prepared as described by Caglieris et al..[27] The compounds **CDn2** (n=6, 7, 8) were synthesized as detailed in the Supporting Information file. The ^{1}H and ^{13}C NMR characterization of all compounds was carried out with a 400 MHz Bruker Avance spectrometer. When appropriate, quantitative ^{13}C NMR spectra of several compounds were obtained by inverse gated decoupling sequences to avoid NOE effects. ESI-MS mass spectra of compounds **CDn1** (n=6, 7, 8) were collected on a Bruker Esquire 3000+ with electrospray ionization source and ion-trap detector using methanol as solvent. All the characterization data are available in the Supporting Information file.

S**ynthesis of CDn3, CDn4 and CDn5 (n=6, 7, 8)**

In a typical preparation **CDn2** (1.0 mmol) and benzophenone (60.7 mg, 0.3 mmol) were dissolved with 20 mL of MeOH (see also Note 1) in a quartz glass test tube. An excess of 2-mercaptoethanol (2.50 g, 32.0 mmol, synthesis of **CDn3**) or 1-thioglycerol (3.46 g, 32.0 mmol, synthesis of **CDn4**) or 3-mercaptopropionic acid (3.40 g, 32.0 mmol, synthesis of **CDn5**) was added. The solution was stirred overnight under N_2 atmosphere at 25 °C under UV-light irradiation (2 lamps, Philips TL 8W BLB). After removing the solvent under reduced pressure, the material was washed with MeCN (5×30 mL) in order to remove the unreacted thiols. A further purification was obtained by column chromatography (SiO_2) initially eluting with $CHCl_3$ (or EtOAc) in order to eliminate the residual impurities and finally eluting with MeOH for the recovery of the product. After the evaporation of the solvent **CDn3, CDn4 and CDn5** compounds were obtained as transparent viscous materials with good yields (≈70-80 %).

Synthesis of CDn6 and CDn7 (n=6, 7, 8)

For the synthesis of **CDn6** (**CDn7**) 0.50 mmol of **CDn3** (**CDn4**) were dissolved in 25 mL of MeOH followed by the addition of an excess of 4-(propargyloxy)-TEMPO (1.26 g, 6.0 mmol), 0.5 mL of Et_3N and 50.0 mg of CuI. The mixture was stirred at 50 °C for 24 h under N_2 atmosphere. After removing the solvent under reduced pressure the residual 4-(propargyloxy)-TEMPO was recovered by washing the solid with EtOAc. The partially purified solid was then dissolved in few mL of MeOH containing 0.5 mL of concentrated NH_4OH(aq). The product (**CDn6** or **CDn7**) was recovered with a quantitative yield as reddish solid after eliminating the copper salts by column chromatography (SiO_2) using MeOH as eluent and final solvent evaporation.

Synthesis of CDn8 (n=6, 7, 8)

An excess of 4-(propargyloxy)-TEMPO (1.26 g, 6.0 mmol) was added to a solution of **CDn5** (0.50 mmol) in 25 mL of MeOH. Then, sodium methoxide (648.4 g, 12.0 mmol) was added at 0°C. After 10 min 0.5 mL of Et_3N and 50.0 mg of CuI were added. The mixture was stirred for 24h at 50°C under N_2 atmosphere. The removal of copper salts and the recovery of **CDn8** as sodium salt was carried out with a procedure similar to the one described for **CDn6** and **CDn7**. The final derivative **CDn8** as ammonium salt was obtained in this way: the original sodium salt was dissolved in a minimum amount of water. The solution was chilled at 0°C. An orange solid was precipitated at 0°C after reducing the pH (final value: 2) by the addition of HCl (aq, 1M). The solid was recovered by centrifugation and washed with 5 mL of cold HCl (aq, 1M) (3 times) and 5 mL of deionized water (3 times). The material was finally dispersed in cold (0°C) deionized water (5 mL) and dissolved by the dropwise addition of concentrated NH_4OH(aq). The clear solution was finally frozen and then freeze-dried to provide the desired compound in quantitative yield.

DC-SQUID magnetometry

Temperature dependent susceptibility and isothermal magnetization measurements were carried out by a commercial DC-SQUID magnetometer MPMS Quantum Design on **CDn1** (n=6, 7, 8) derivatives as powder samples. Both the molar susceptibility as a function of temperature (2 – 300 K) and the isothermal magnetization (0 – 5.5 T) at several temperatures were measured.

Relaxivity measurements

The measurements of the longitudinal relaxation time (T_1) were obtained at 300 K on a 400 MHz (9.4 T) Bruker Avance spectrometer with a standard inversion–recovery (180–t–90) sequence. The time interval (t) was changed between 1 ms and 24 s (number of experiments NE = 22) and the repetition time was set at 40 s. The compounds were dissolved in DMSO-d_6 / H_2O (9:1 v:v) or D_2O / H_2O (9:1 v:v) according to Table 1. The integrals of the water peak in the ^{1}H spectra vs. the corresponding time t, were used to calculate the T_1 values by means of the supplied XWINNMR Bruker software, fitting the data with a mono-exponential function.

In Vivo MRI Experiments

All animal experiments were approved by the Animal Health Welfare and Ethics Committee of University of Eastern Finland. Briefly, female Wistar rats (N=15, 190 – 370 g, Envigo) were implanted with 10^6 C6 glioma cells (ECACC/Sigma Aldrich) to stereotactic coordinates of 1 mm caudal from bregma, 2 mm to the right of sagittal suture and 2 mm below the top of bregma through a burr hole.[36,37]

MRI experiments were performed at 9.4 T (Agilent, Santa Clara, US) using a volume coil transmitter/4-channel surface coil receiver pair (Rapid Biomedical, Rimpar, Germany) on days 11-18 after implantation. During the experiments, the animals were under isoflurane anesthesia (5% induction, 1-2% upkeep, 70:30 N_2:O_2 gas mixture at 2 L/min) with physiological monitoring (60-80 breaths per minute, 37 degrees Celsius). Axial (field of view 32x32 mm^2 covered with 128x64 data matrix and eight 1 mm slices unless stated otherwise) multi-slice T_1 (inversion-recovery FLASH with repetition time of 7.8 ms and echo time of 3.9 ms, flip angle 10 degrees, twelve 1 mm slices, 12 inversion times between 5 and 5500 ms, 10 s recovery delay) and T_2 (multi spin-echo with 16 echo times from 8.1 to 129.8 ms, repetition time of 2 s) relaxation maps of the tumor and normal brain were collected before and for up to one hour after the tail vein injection of the contrast agent. Fast gradient echo multi-slice imaging (repetition time 156 ms, echo time 4.5 ms, flip angle 90 degrees, 256x128 data matrix) was performed during the first ten minutes following CA injection. The final concentration of **CD78**, dissolved to saline, was 0.19 to 0.49 mmol/kg (injected sample concentration varying between 33 and 100 mM) (n=10). For Gd(DTPA), final concentration was 0.1 to 0.29 mmol/kg (n=8). Furthermore, two animals received an injection of TEMPOL dissolved to saline at concentration 1.6 mmol/kg. To minimise the number of used animals, some animals received injections of two different contrast agents (**CD78** + Gd or TEMPOL + Gd) during the same MRI experiment. In these cases, there was a delay of at least 75 minutes between injections. All relaxation maps were calculated as monoexponential fits in Matlab (Mathworks, Natick, US) and regions of interest from tumor and normal brains were analysed.

Acknowledgements

In vivo experiments were partially funded by the Academy of Finland (project grant no. 286895) and TEKES/EU Regional Development Fund (no. 4298/31/2014).

Keywords: cyclodextrin • thiol-ene reaction • nitroxides • magnetic resonance imaging • glioma

[1] S. C. Bushong, G. Clarke, *Magnetic Resonance Imaging: Physical and Biological Principles*, Fourth edition, Elsevier **2015**.

[2] L. Helm, A. E. Merbach, É. Tóth, *The Chemistry of Contrast Agents in Medical Magnetic Resonance Imaging*, Second edition, Wiley **2013**.

[3] P. Caravan, J. J. Ellison, T. J. McMurry, R. B. Lauffer, *Chem. Rev.* **1999**, *99 (9)*, 2293-2352.

[4] P. Marckmann, L. Skov, K. Rossen, A. Dupont, M. Brimnes Damholt, J. Goya Heaf and H. S. Thomsen, *J. Am. Soc. Nephrol.* **2006**, *17 (9)*, 2359-2362.

[5] A. Rajca, Y. Wang, M. Boska, J. T. Paletta, A. Olankitwanit, M. A. Swanson, D. G. Mitchell, S. S. Eaton, G. R. Eaton, S. Rajca, *J. Am. Chem. Soc.* **2012**, *134 (38)*, 15724-15727.

[6] M. Soikkeli, K. Sievänen, J. Peltonen, T. Kaasalainen, M. Timonen, P. Heinonen, S. Rönkkö, V.-P. Lehto, J. S. Kavakka, S. Heikkinen, *RSC Adv.* **2015**, *5*, 15507-15510.

[7] M. Soikkeli, K. Horkka, J. O. Moilanen, M. Timonen, J. Kavakka, S. Heikkinen, *Molecules* **2018**, *23(5)*, 1034.

[8] K.-I. Matsumoto, F. Hyodo, A. Matsumoto, A. P. Koretsky, A. L. Sowers, J. B. Mitchell, M. C. Krishna, *Clin. Cancer Res.* **2006**, *12(8)*, 2455-2462.

[9] Z. Zhelev, R. Bakalova, I. Aoki, K.-I. Matsumoto, V. Gadjeva, K. Anzai, I. Kanno, *Mol. Pharmaceutics* **2009**, *62*, 504-512.

[10] Z. Zhelev, R. Bakalova, I. Aoki, K.-I. Matsumoto, V. Gadjeva, K. Anzai, I. Kanno, *Chem. Commun.* **2009**, 53-55.

[11] Z. Zhelev, I. Aoki, V. Gadjeva, B. Nikolova, R. Bakalova, T. Saga, *Eur. J. Cancer* **2013**, 49(6), 1467-1478.

[12] M. A. Sowers, J. R. McCombs, Y. Wang, J. T. Paletta, S. W. Morton, E. C. Dreaden, M. D. Boska, M. F. Ottaviani, P. T. Hammond, A. Rajca, J. A. Johnson, *Nat. Commun.* **2014**, *5*, 5460.

[13] L. Huang, C. Yan, D. Cui, Y. Yan, X. Liu, X. Lu, X. Tan, X. Lu, J. Xu, Y. Xu, R. Liu, *Macromol. Biosci.* **2015**, *15(6)*, 788-798.

[14] M. Dharmarwardana, A. F. Martins, Z. Chen, P. M. Palacios, C. M. Nowak, R. P. Welch, S. Li, M. A. Luzuriaga, L. Bleris, B. S. Pierce, A. Dean Sherry, J. J. Gassensmith, *Mol. Pharm.* **2018**, *158*, 2973-2983.

[15] K. Morishita, S. Murayama, T. Araki, I. Aoki, S. Karasawa, *J. Org. Chem.* **2016**, *81(18)*, 8351-8362.

[16] H. V.-T. Nguyen, Q. Chen, J. T. Paletta, P. Harvey, Y. Jiang, H. Zhang, M. D. Boska, M. F. Ottaviani, A. Jasanoff, A. Rajca, J. A. Johnson, *ACS Cent. Sci.* **2017**, *37*, 800-811.

[17] S. Garmendia, D. Mantione, S. Alonso-de Castro, C. Jehanno, L. Lezama, J. L. Hedrick, D. Mecerreyes, L. Salassa, H. Sardon, *Polym. Chem.* **2017**, *8*, 2693-2701.

[18] M. Hou, X. Lu, Z. Zhang, Q. Xia, C. Yan, Z. Yu, Y. Xu, R. Liu, *ACS Appl. Mater. Interfaces* **2017**, 9(51), 44316-44323.

[19] H. V.-T. Nguyen, A. Detappe, N. M. Gallagher, H. Zhang, P. Harvey, C. Yan, C. Mathieu, M. R. Golder, Y. Jiang, M. F. Ottaviani, A. Jasanoff, A. Rajca, I. Ghobrial, P. P. Ghoroghchian, J. A. Johnson, *ACS Nano* **2018**, *12(11)*, 11343-11354.

[20] E. Mauri, E. Micotti, A. Rossetti, L. Melone, S. Papa, G. Azzolini, S. Rimondo, P. Veglianese, C. Punta, F. Rossi, A. Sacchetti, *Soft Matter* **2018**, *14*, 558-565.

[21] G. Gil Alvaradejo, H. V.-T. Nguyen, P. Harvey, N. M. Gallagher, D. Le, M. F. Ottaviani, A. Jasanoff, G. Delaittre, J. A. Johnson, *ACS Macro Lett.* **2019**, *84*, 473-478.

[22] E.M. Martin Del Valle, *Process Biochem.* **2004**, *39(9)*, 1033-1046.

[23] F. Bellia, D. La Mendola, C. Pedone, E. Rizzarelli, M. Saviano, G. Vecchio, *Chem. Soc. Rev.* **2009**, *38* , 2756 -2781.

[24] W.-F. Lai, A. L. Rogach, W.-T. Wong, *Chem. Soc. Rev.* **2017**, *46*, 6379-6419.

[25] A. Biscotti, C. Barbot, L. Nicol, P. Mulder, C. Sappei, M.-H. Roux, I. Déchamps-Olivier, F. Estour, G. Gouhier, *Polyhedron* **2018**, 148, 32-43.

[26] Y. A. Mondjinou, B. P. Loren, C. J. Collins, S.-H. Hyun, A. Demoret, J. Skulsky, C. Chaplain, V. Badwaik, D. H. Thompson, *Bioconjugate Chem.* **2018**, *29(11)*, 3550-3560.

[27] F. Caglieris, L. Melone, F. Canepa, G. Lamura, F. Castiglione, M. Ferro, L. Malpezzi, A. Mele, C. Punta, P. Franchi, M. Lucarini, B. Rossi, F. Trotta, *RSC Adv.* **2015**, *5*, 76133-76140.

[28] F. Caracciolo, P. Carretta, M. Filibian, L. Melone, *J. Phys. Chem. B* **2017**, *121 (12)*, 2584-2593.

[29] F. Caracciolo, A. Lucini Paioni, M. Filibian, L. Melone, P. Carretta, *J. Phys. Chem. B* **2018**, *122 (6)*, 1836-1845.

[30] F. Caracciolo, E. Charlaftis, L. Melone, P. Carretta, *J. Phys. Chem. B* **2019**, *123 (17)*, 3731-3737.

[31] É. Tóth, L. Helm , A. E. Merbach, in *Contrast agents I, Magnetic Resonance Imaging*, (Ed. W. Krause) Springer, **2002**, pp. 62–98

[32] A. B. Lowe, *Polym. Chem.* **2014**, *5*, 4820-4870.

[33] J. Kalpathy-Cramer, E. R. Gerstner, K. E. Emblem, O. C. Andronesi, B. Rosen, *Cancer Res.* **2014**, *74(17)*, 4622–4637.

[34] C. S. Wilcox, A. Pearlman, *Pharm. Rev.* **2008**, *60*, 418-469.

[35] K. M. Donahue, D. Burstein, W. J. Manning, M. L. Gray, *Magn. Reson. Med.* **1994**, *32 (1)*, 66-76.

[36] M. Soikkeli, M. I. Kettunen, R. Nivajärvi, V. Olsson, S. Rönkkö, J. P. Laakkonen, V.-P. Lehto, J. Kavakka, S. Heikkinen, *Contrast Media Mol. I.* **2019**, 5629597.

[37] R. Nivajärvi, V. Olsson, V. Hyppönen, S. Bowen, H. M. Leinonen, H. P. Lesch, J. H. Ardenkjær-Larsen, O.H.J. Gröhn, S. Ylä-Herttuala, M. I. Kettunen, *NMR in Medicine* **2020**, DOI: 10.1002/nbm.4250.

[38] P. R. Ashton, R. Königer, J. F. Stoddart, *J. Org. Chem.* **1996**, *61(3)*, 903–908.

[39] A. Bogdan, D. T. McQuade, *Beilstein J. Org. Chem.* **2009**, *5*, 17.

[40] O. Udochukwu Akakuru, M. Zubair Iqbal, M. Saeed, C. Liu, T. Paunesku, G. Woloschak, N. S. Hosmane, A. Wu, *Bioconjugate Chemistry* **2019**, *30* (9), 2264-2286.

[41] H. Lee, A. Shahrivarkevishahi, J. L. Lumata, M. A. Luzuriaga, L. M. Hagge, C. E. Benjamin, O. R. Brohlin, C. R. Parish,b H. R. Firouzi, S. O. Nielsen, L. L. Lumata, J. J. Gassensmith, *Chem. Sci.* **2020**,*11*, 2045-2050.

[42] Figure S32 shows a comparison of the isothermal magnetization data for **CD71** and **CD76** as a function of H/T (at T=2 K). We remark that the two datasets are almost superposed. Further, a linear fit on the T-dependent inverse molar magnetic susceptibility $1/\chi_m$ measured by applying a magnetic field of 50 mT gives an effective moment μ_{eff}=4.240(3) μ_B fully in agreement with the one found for **CD71** sample (μ_{eff}=4.262(1) μ_B) (fit data not shown). These results indicate that the magnetic properties of the final ORCA are not affected by the functionalization on the CD large rim. For this reason DC-SQUID measurements were essentially limited to the set of compounds **CDn1** (n=6, 7, 8).

Entry for the Table of Contents

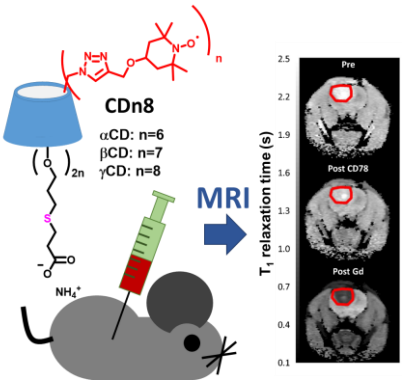

Soluble in water: A family of water soluble cyclodextrin-based polynitroxides have been synthesized by a straightforward combination of thiol-ene and copper(I)-catalized alkyne-azide “click reactions”. These compounds have been tested as contrast agents for the *in vivo* detection of glioma tumor in animal models.

Supporting Information

Cyclodextrin-based organic radical contrast agents for *in vivo* imaging of glioma

Lucio Melone*[a,b], Alice Bach[c], Gianrico Lamura[d], Fabio Canepa[d,e] Riikka Nivajärvi[f], Venla Olsson[g] and Mikko Kettunen*[e]

Table of contents

Synthesis of CDn2 (n=6, 7, 8)

2 mmol of dried† **CDn0** (2.246 g for n=6, 2.620 g for n=7, and 2.995 g for n=8) were dissolved in 30 mL of anhydrous DMF‡ in a 100 mL two necked round bottom flask. After cooling the solution at 0°C, an excess of NaH (5 g, ~60% in mineral oil, 125 mmol) was added and the misxture was stirred at 0°C under a slow flow of N_2 for 30 min. 5 mL of allylbromide (~58 mmol) were added dropwise. The mixture was stirred under N_2 atmosphere for 8 h at 0°C, then overnight at room temperature. The residual NaH was eliminated by the slow addition of water at 0°C and under N_2 flow. The organic components were extracted with EtOAc from the aqueous phase. After the solvent evaporation with a rotary evaporator, the residual material still contained the mineral oil and the residual DMF. The first was mainly eliminated by the addition of hexane (25 mL×3 times) into the flask followed by a slow decantation of the surnatant. The second was mainly eliminated by washing the residual material with water (25 mL×3 times). The obtained sticky solid was dissolved in 50 mL of EtOAc and dried with anhydrous Na_2SO_4. The solution was concentrated under rotary evaporation. The purified product was obtained from column chromatography (SiO_2), first eluting with hexane in order to remove residual traces of mineral oil, then eluting with hexane/EtOAc 1:1 (v:v) to recover the product as a pale yellow sticky solid. The yields are generally around to 80%.

† Overnight at 105°C.

‡ Dried with CaH_2 for 48 h before use.

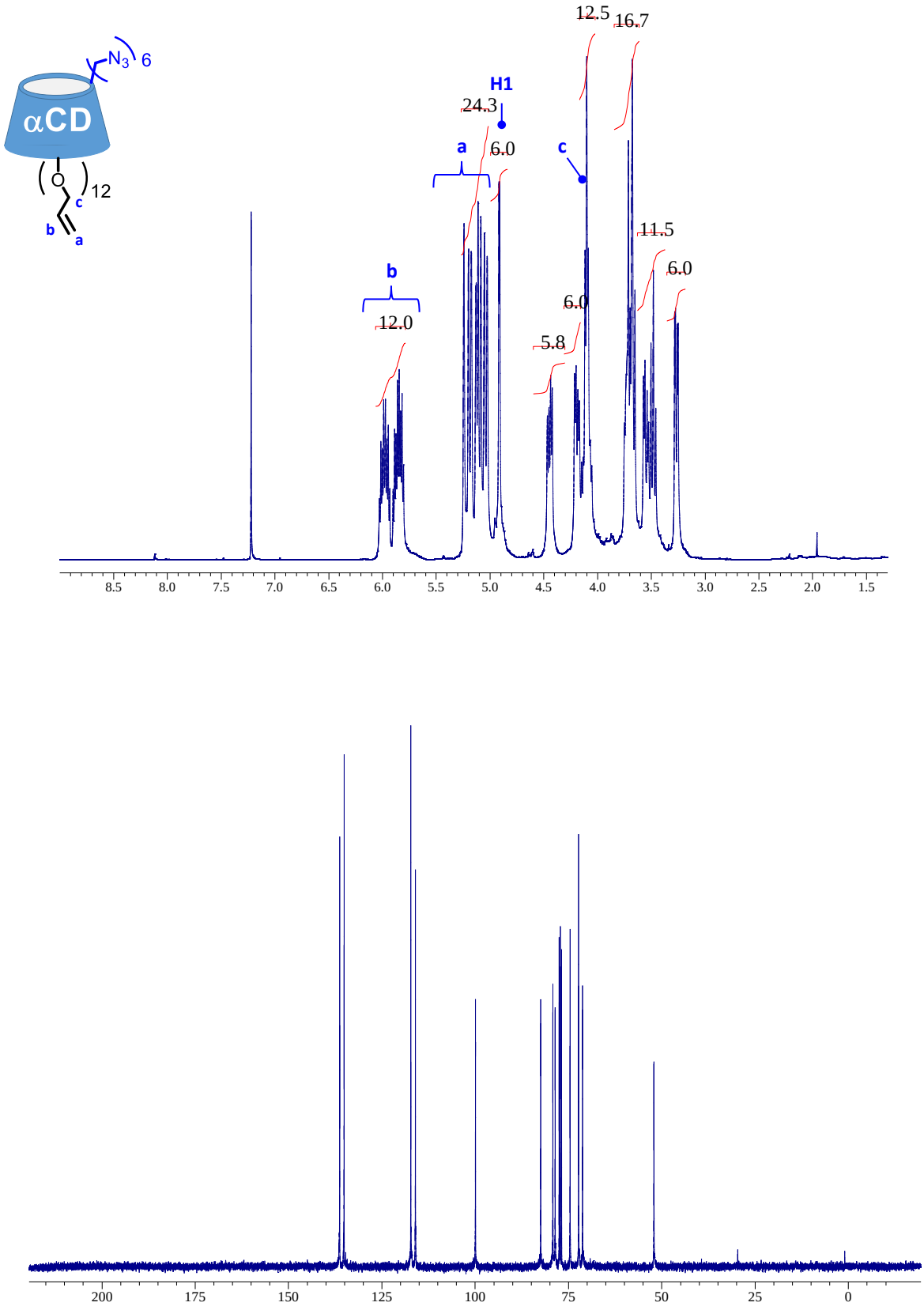

Fig.S1. ^{1}H and ^{13}C NMR spectra of **CD62**. Solvent: $CDCl_3$.

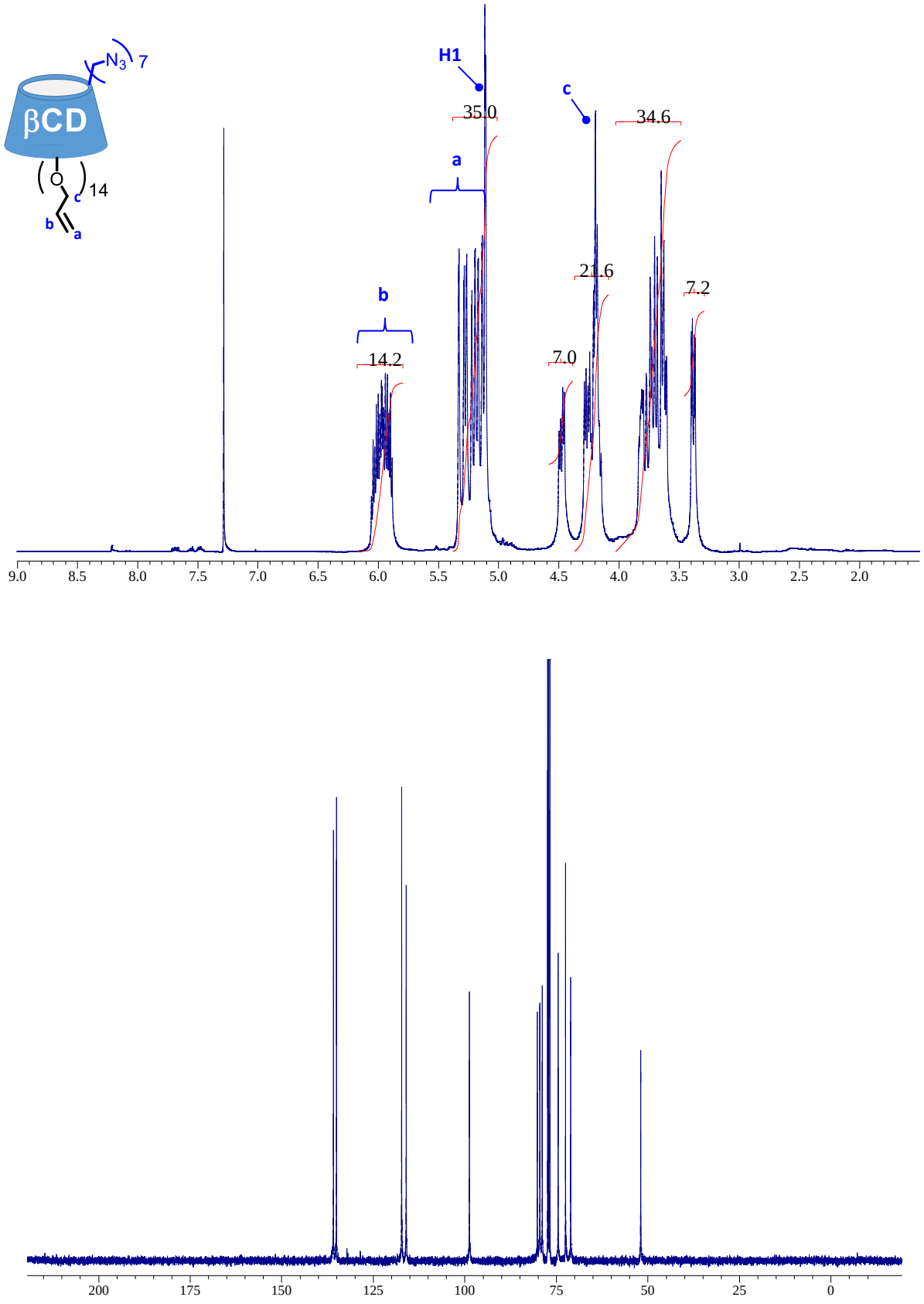

Fig.S2. ^{1}H and ^{13}C NMR spectra of **CD72**. Solvent: $CDCl_3$.

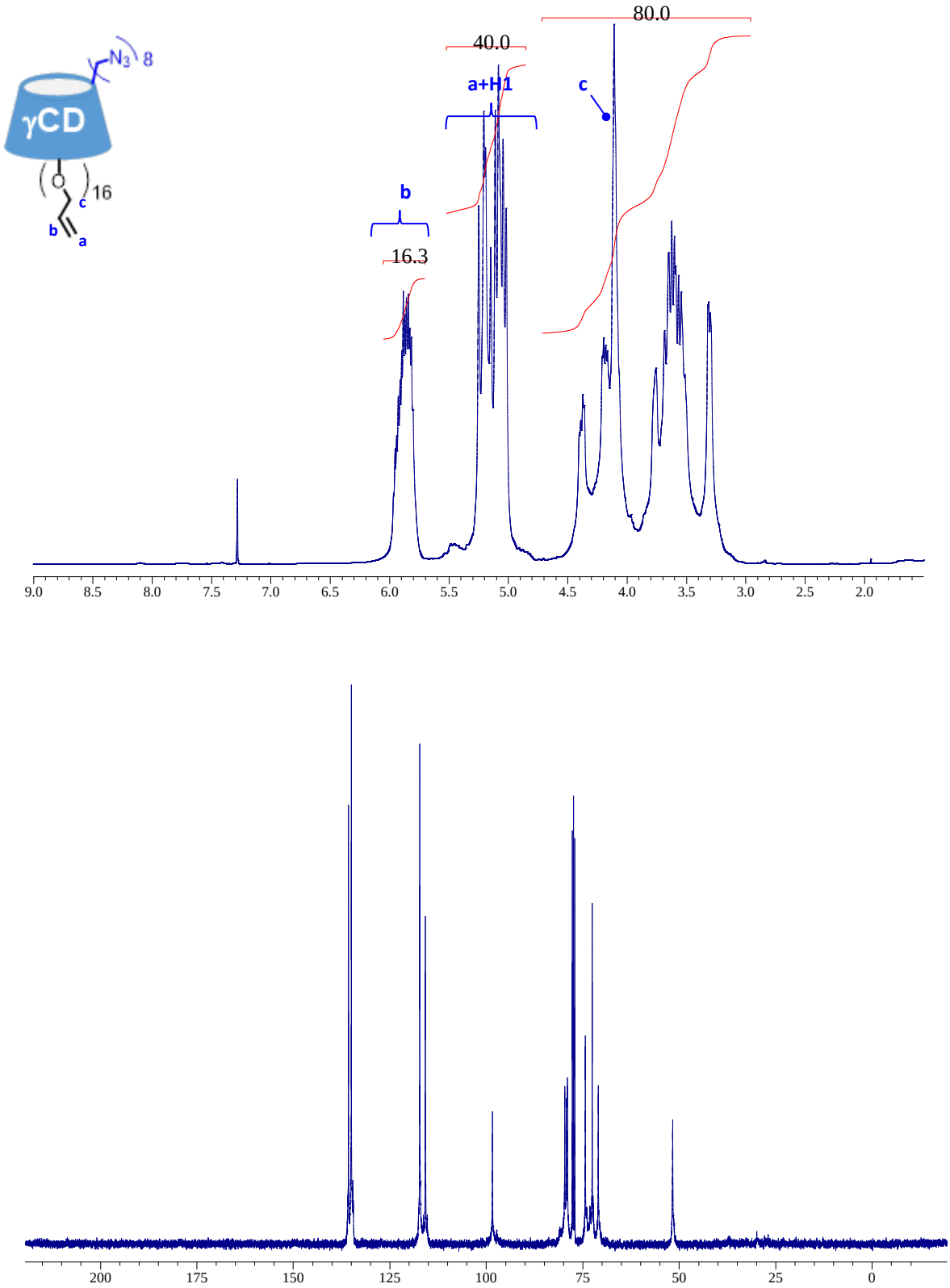

Fig.S3. ^{1}H and ^{13}C NMR spectra of **CD82**. Solvent: $CDCl_3$.

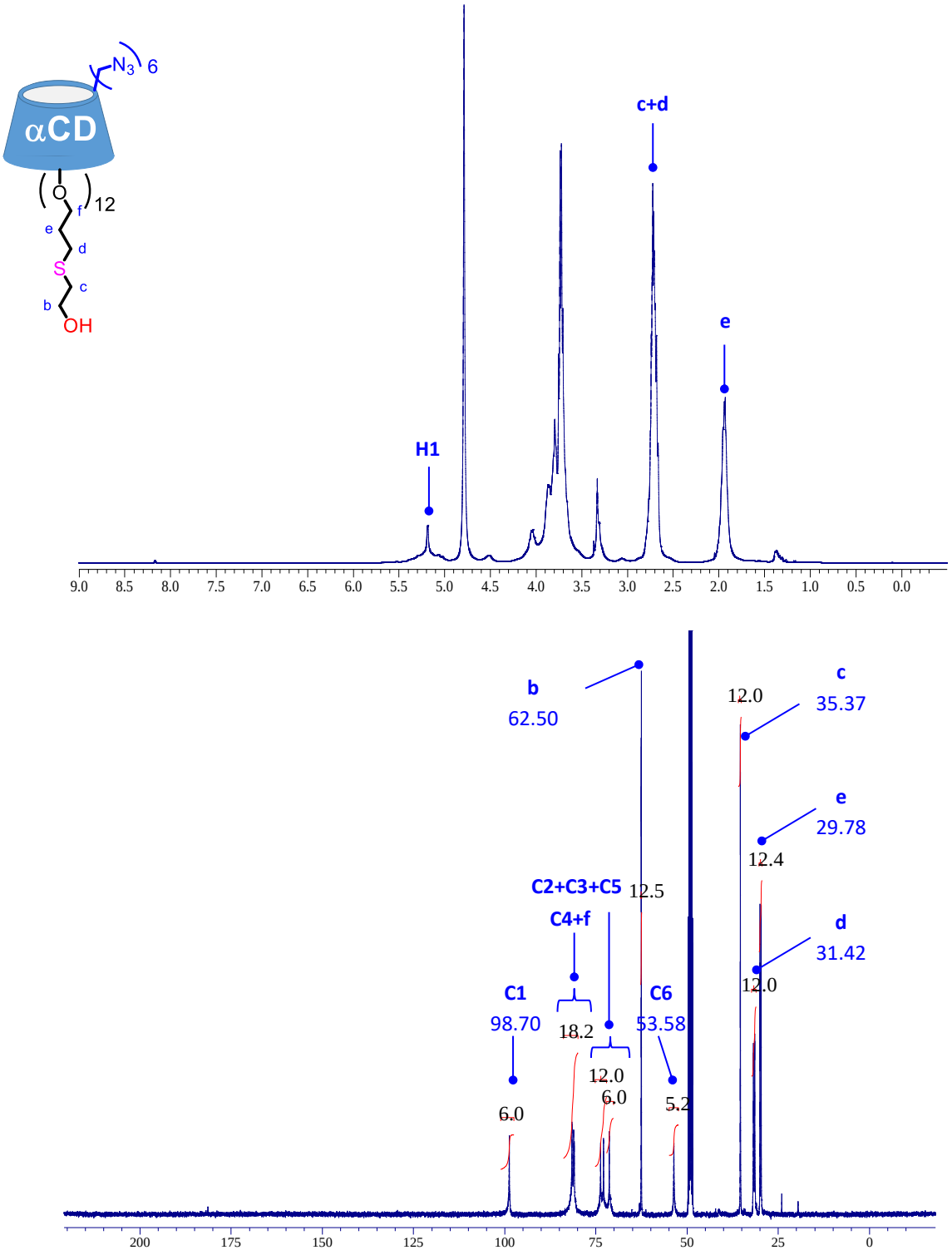

Fig.S4. ^{1}H and Inverse-Gated ^{13}C NMR spectra of **CD63**. Solvent: methanol-d_4.

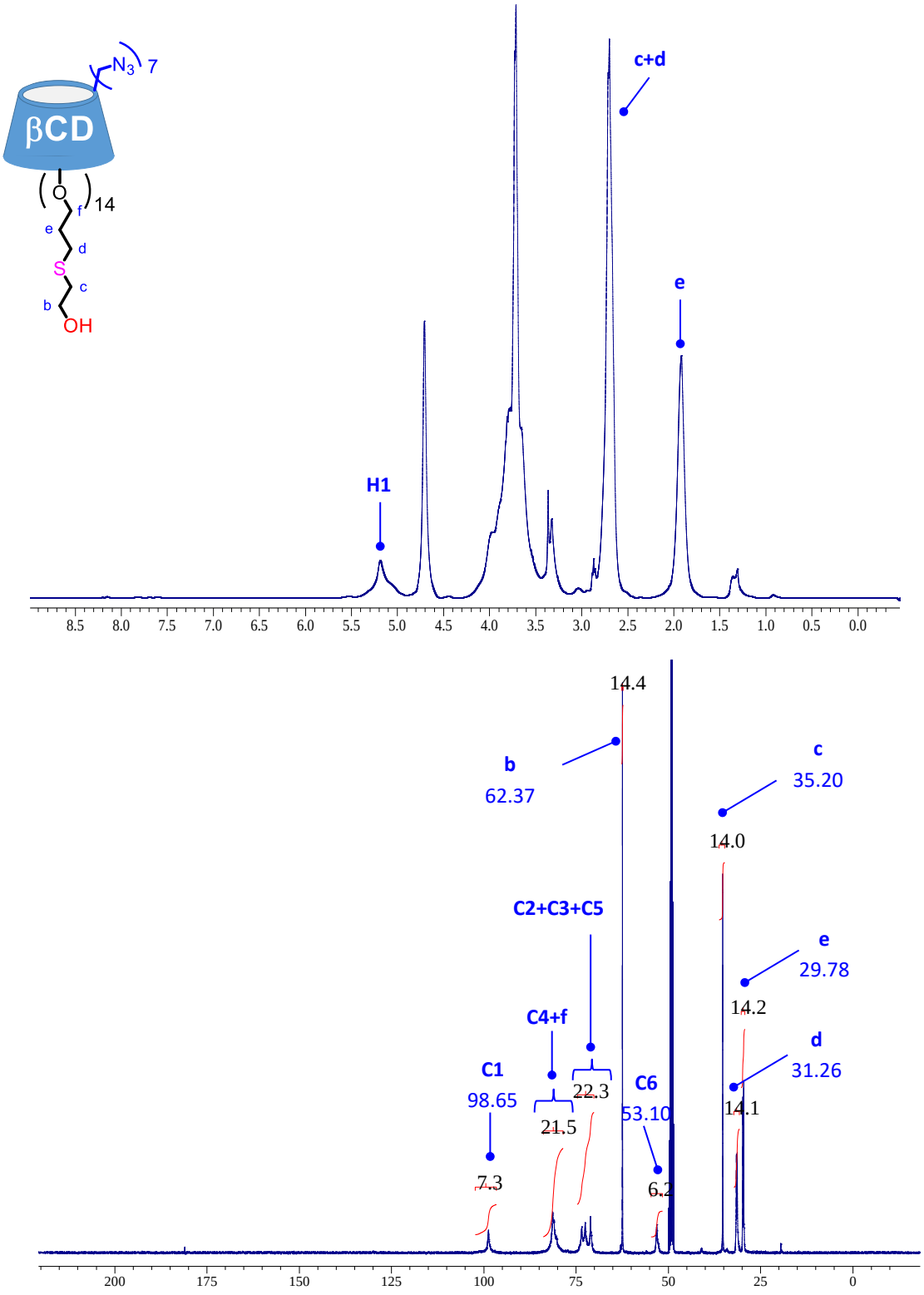

Fig.S5. ^{1}H and Inverse-Gated ^{13}C NMR spectra of **CD73**. Solvent: methanol-d_4.

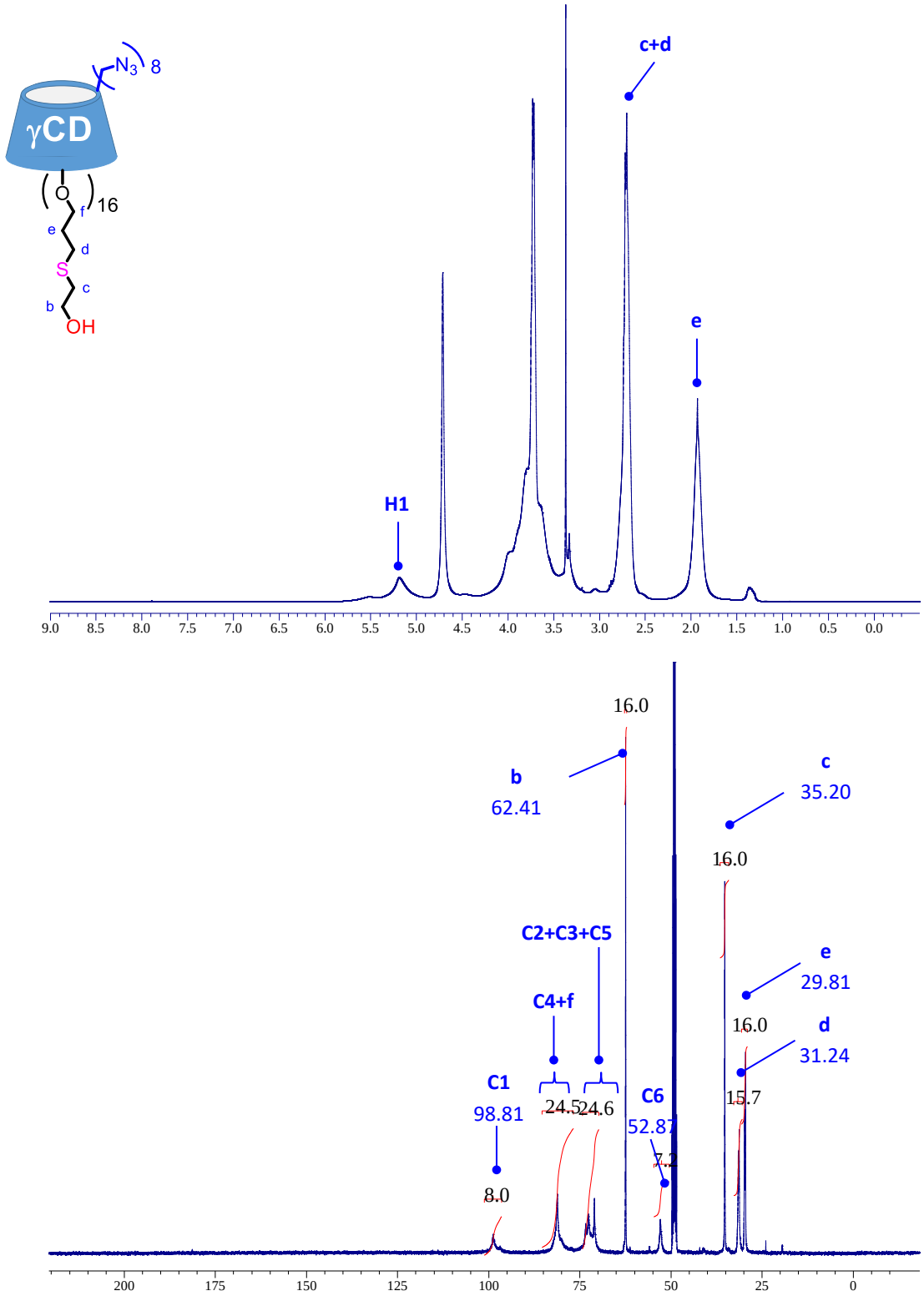

Fig.S6. ^{1}H and Inverse-Gated ^{13}C NMR spectra of **CD83**. Solvent: methanol-d_4.

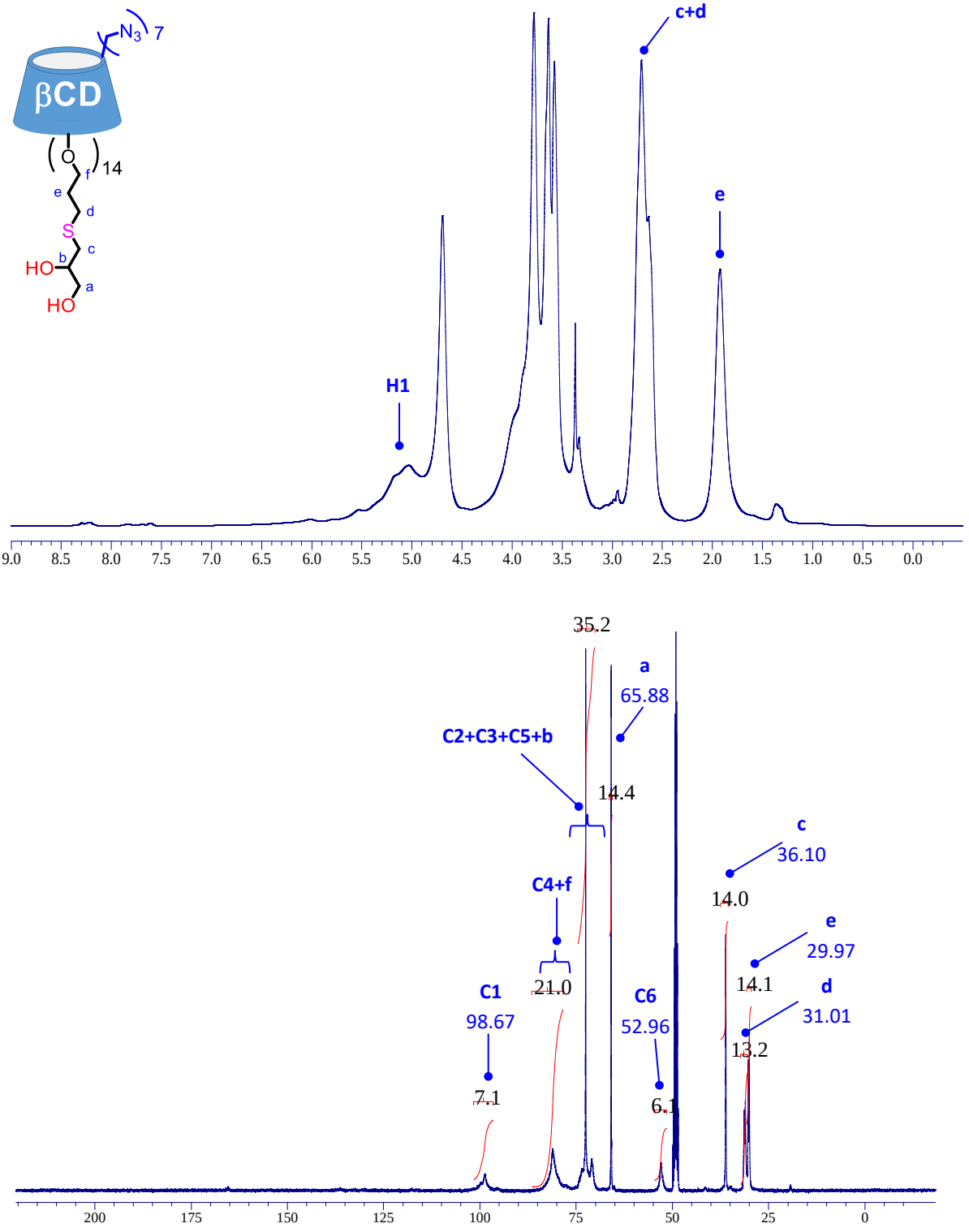

Fig.S7. ^{1}H and Inverse-Gated ^{13}C NMR spectra of **CD74**. Solvent: methanol-d_4.

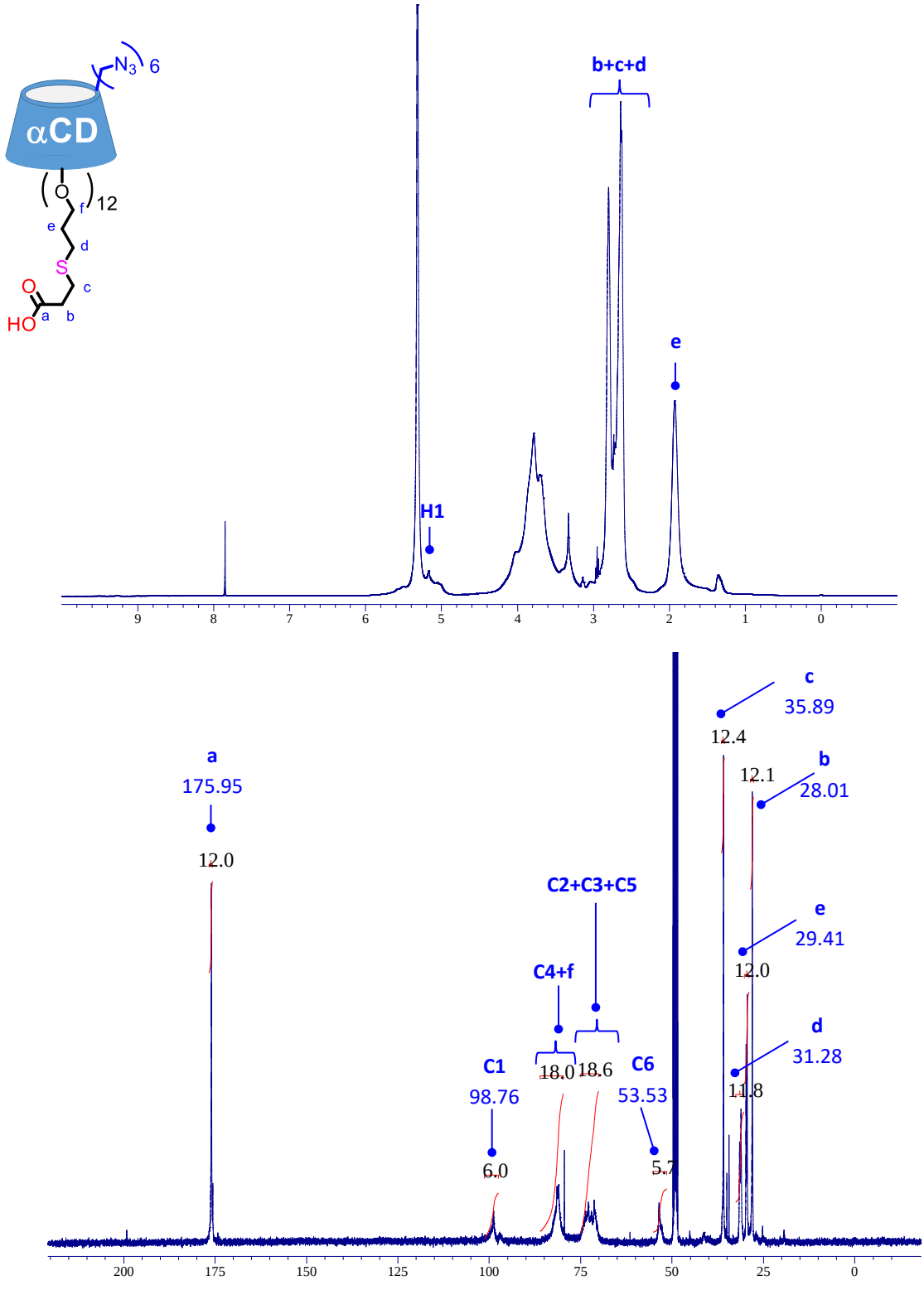

Fig.S8. ^{1}H and Inverse-Gated ^{13}C NMR spectra of **CD65**. Solvent: methanol-d_4.

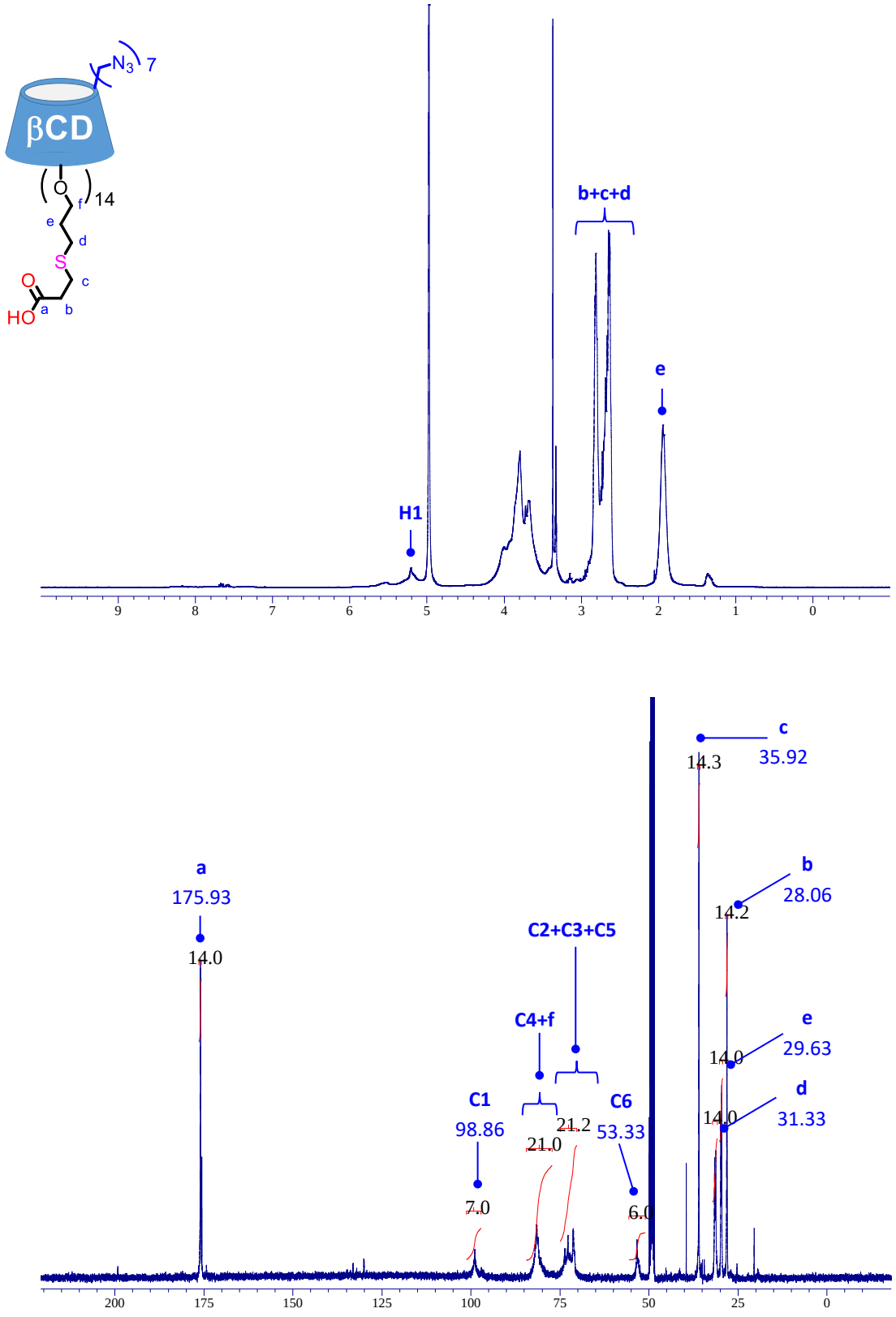

Fig.S9. ^{1}H and Inverse-Gated ^{13}C NMR spectra of **CD75**. Solvent: methanol-d_4.

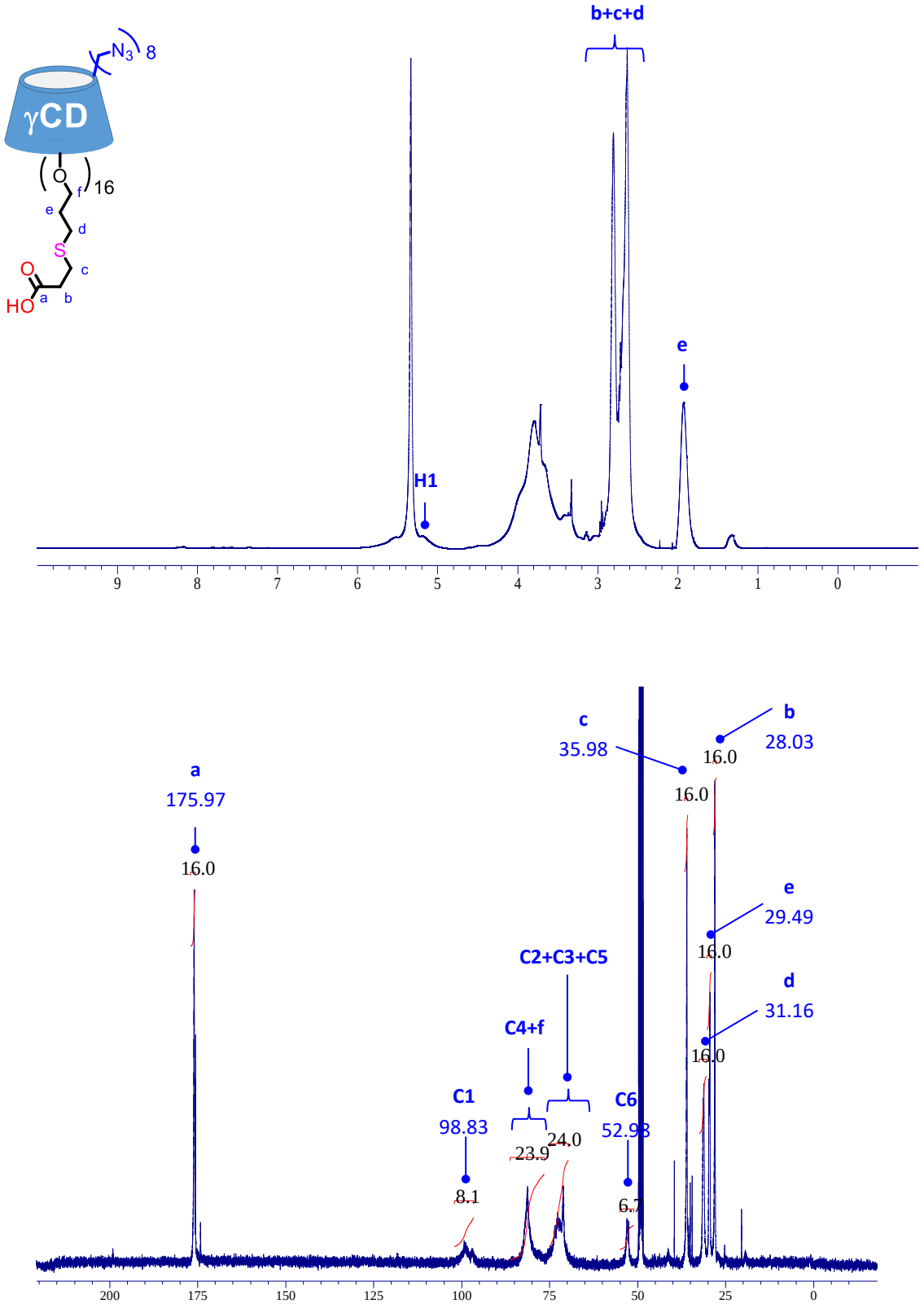

Fig.S10. ^{1}H and Inverse-Gated ^{13}C NMR spectra of **CD85**. Solvent: methanol-d_4.

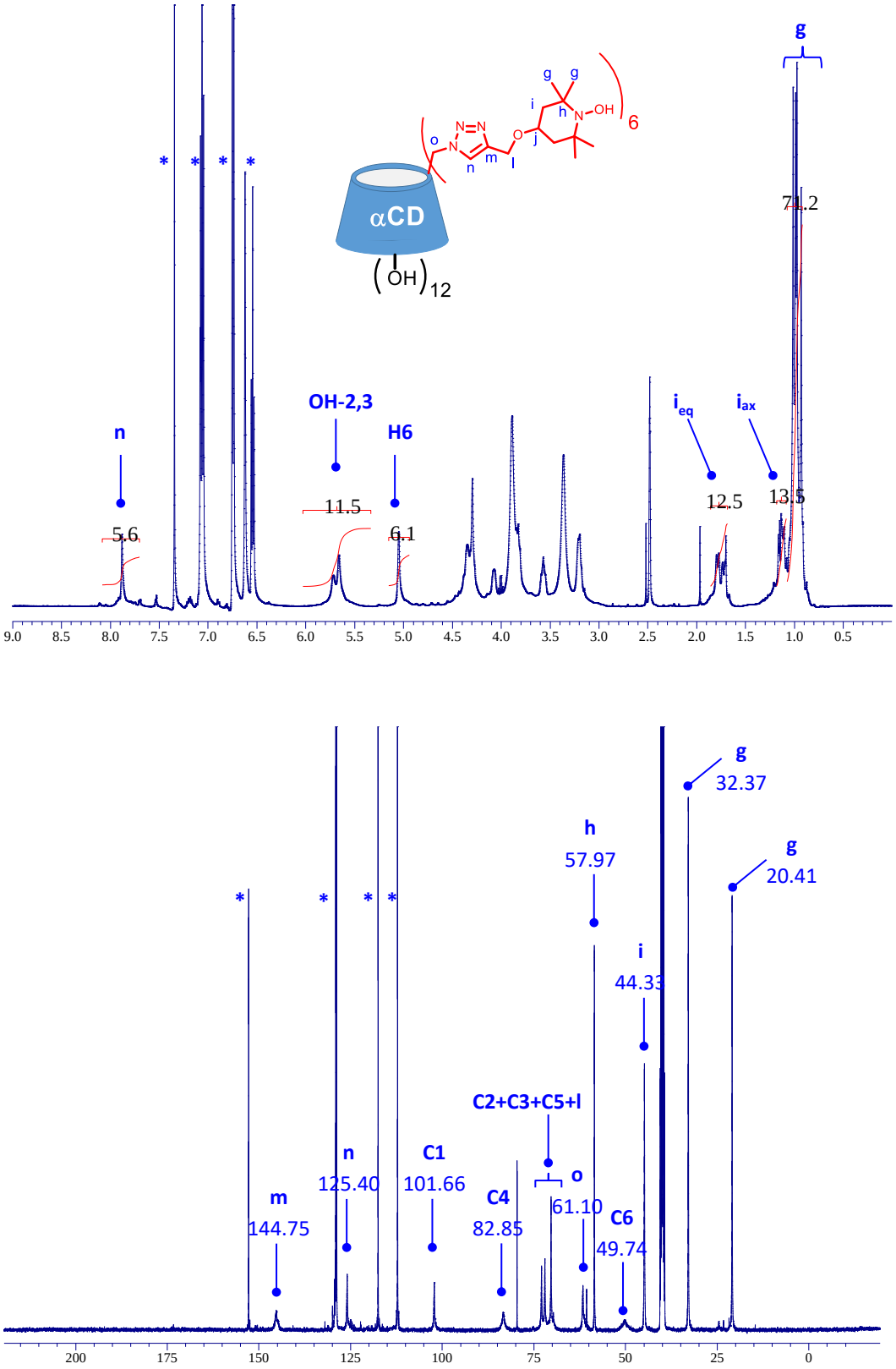

Fig.S11. ^{1}H and ^{13}C NMR spectra of **CD61** after the addition of phenylhydrazine(*). Solvent: DMSO-d_6.

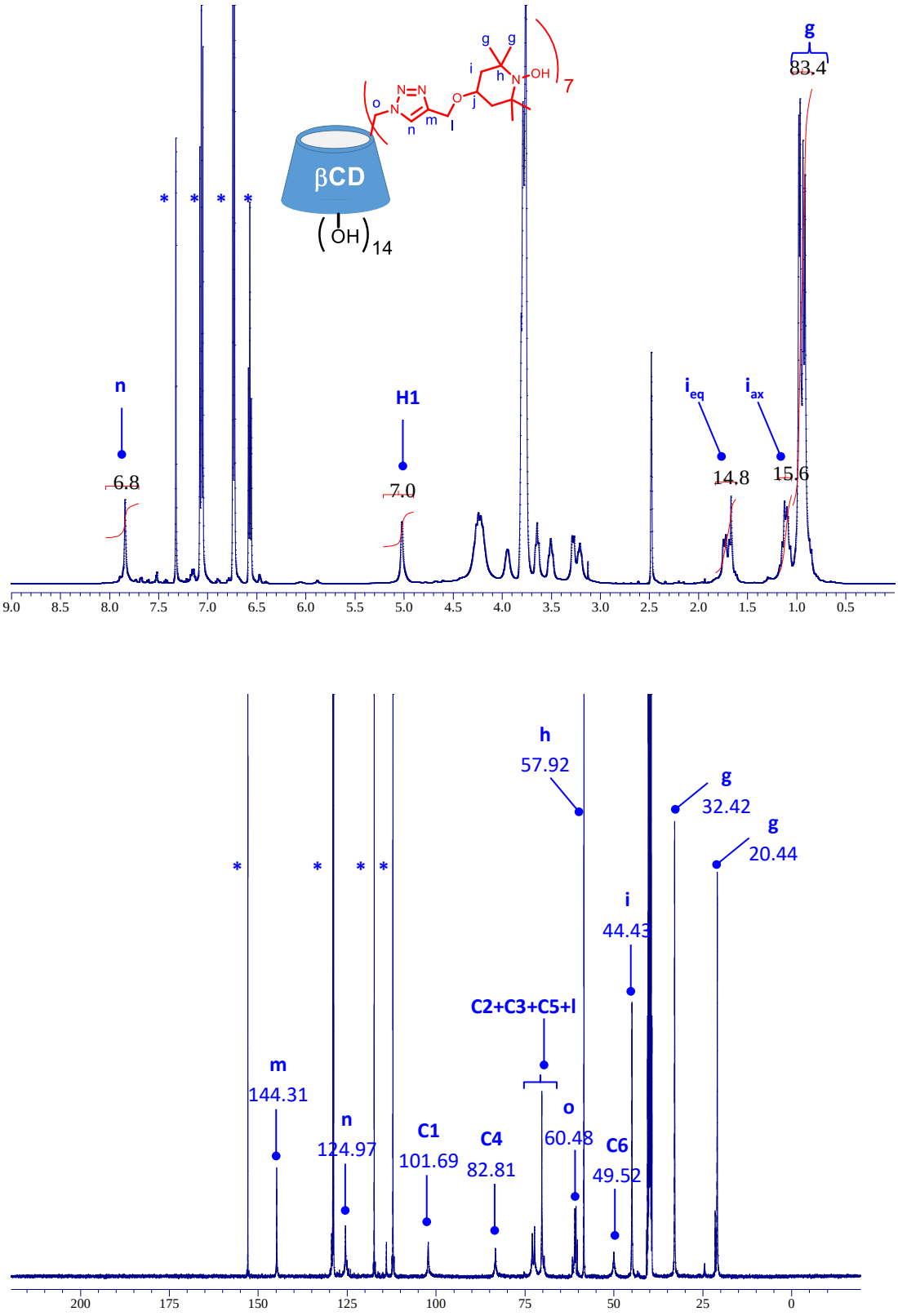

Fig.S12. ^{1}H and ^{13}C NMR spectra of **CD71** after the addition of phenylhydrazine (*). Solvent: DMSO-d_6. NOTE: the ^{1}H NMR spectrum was recorded after the addition of 1 drop of D_2O.

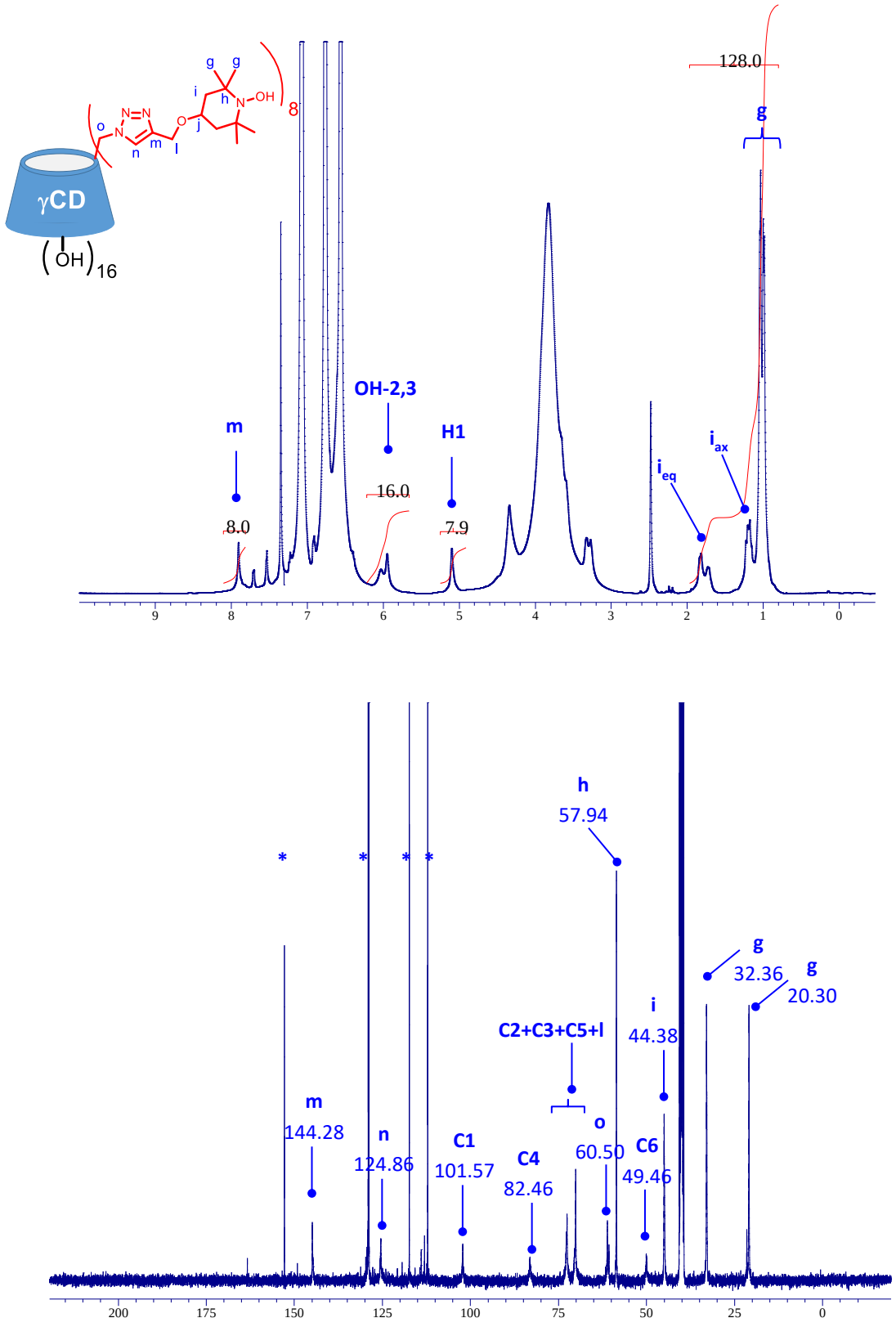

Fig.S13. ^{1}H and ^{13}C NMR spectra of **CD81** after the addition of phenylhydrazine (*). Solvent: DMSO-d_6.

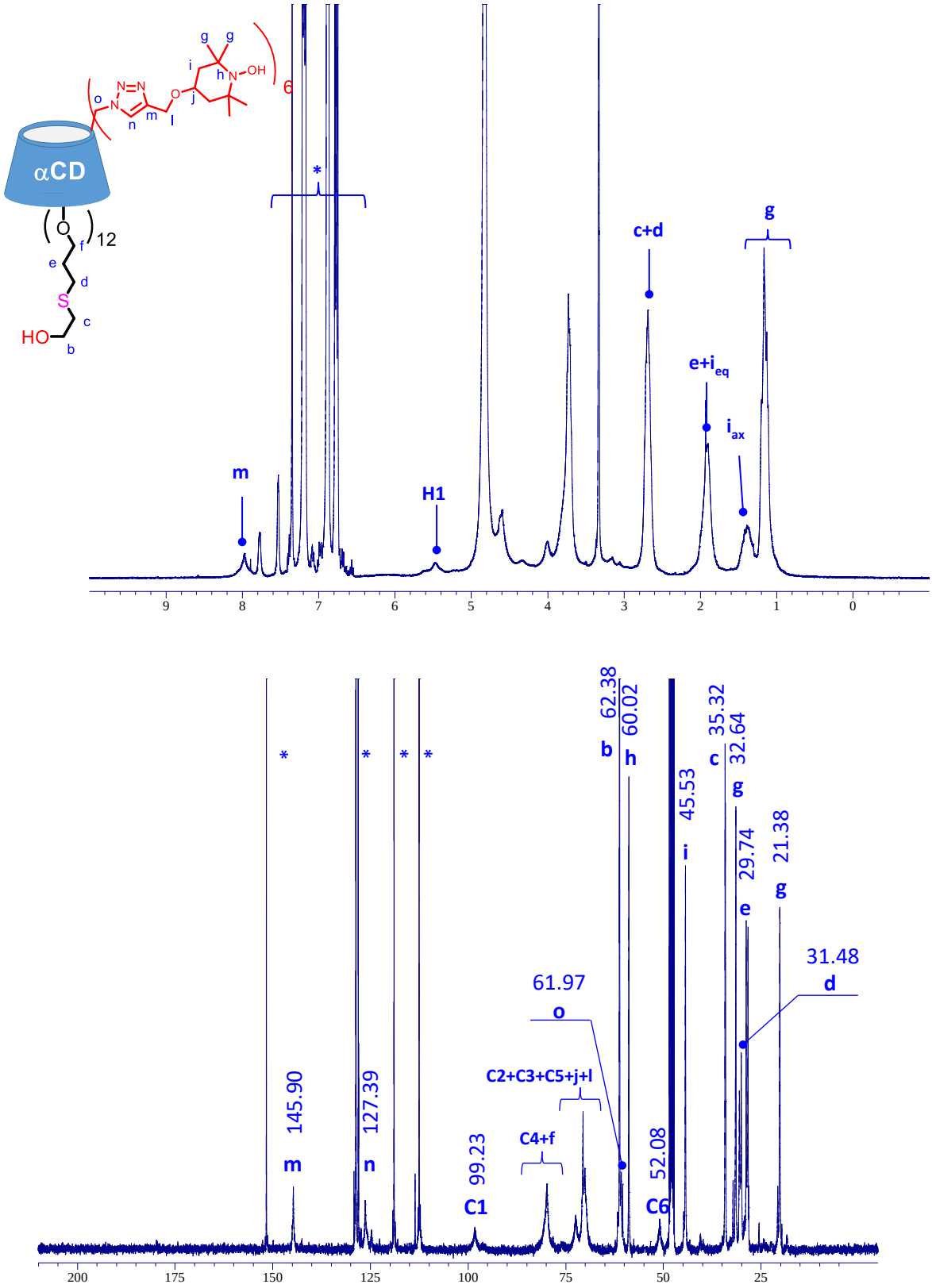

Fig.S14. ^{1}H and ^{13}C NMR spectra of **CD66** after the addition of phenylhydrazine (*). Solvent: methanol-d_3.

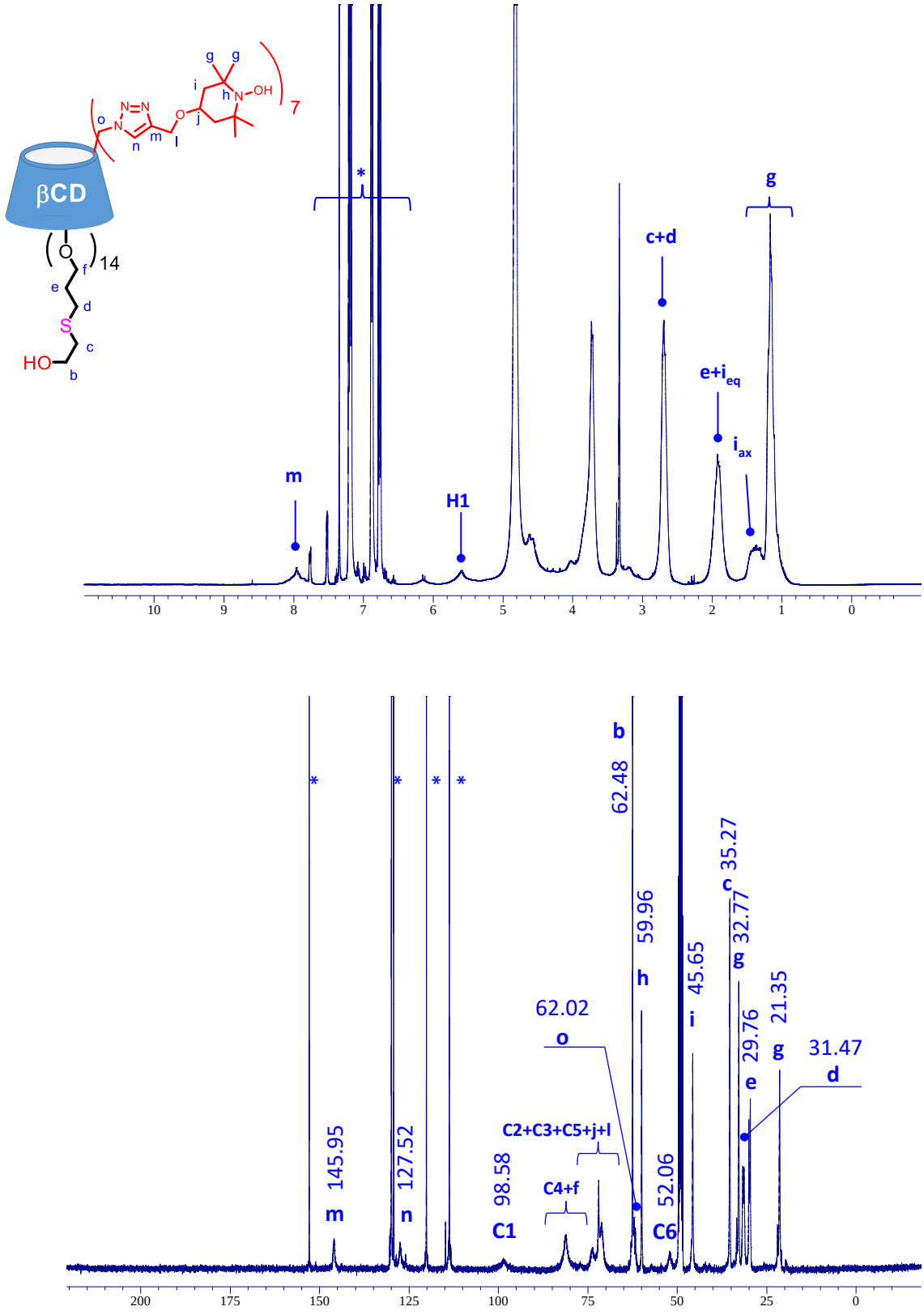

Fig.S15. ^{1}H and ^{13}C NMR spectra of **CD76** after the addition of phenylhydrazine (*). Solvent: methanol-d_3.

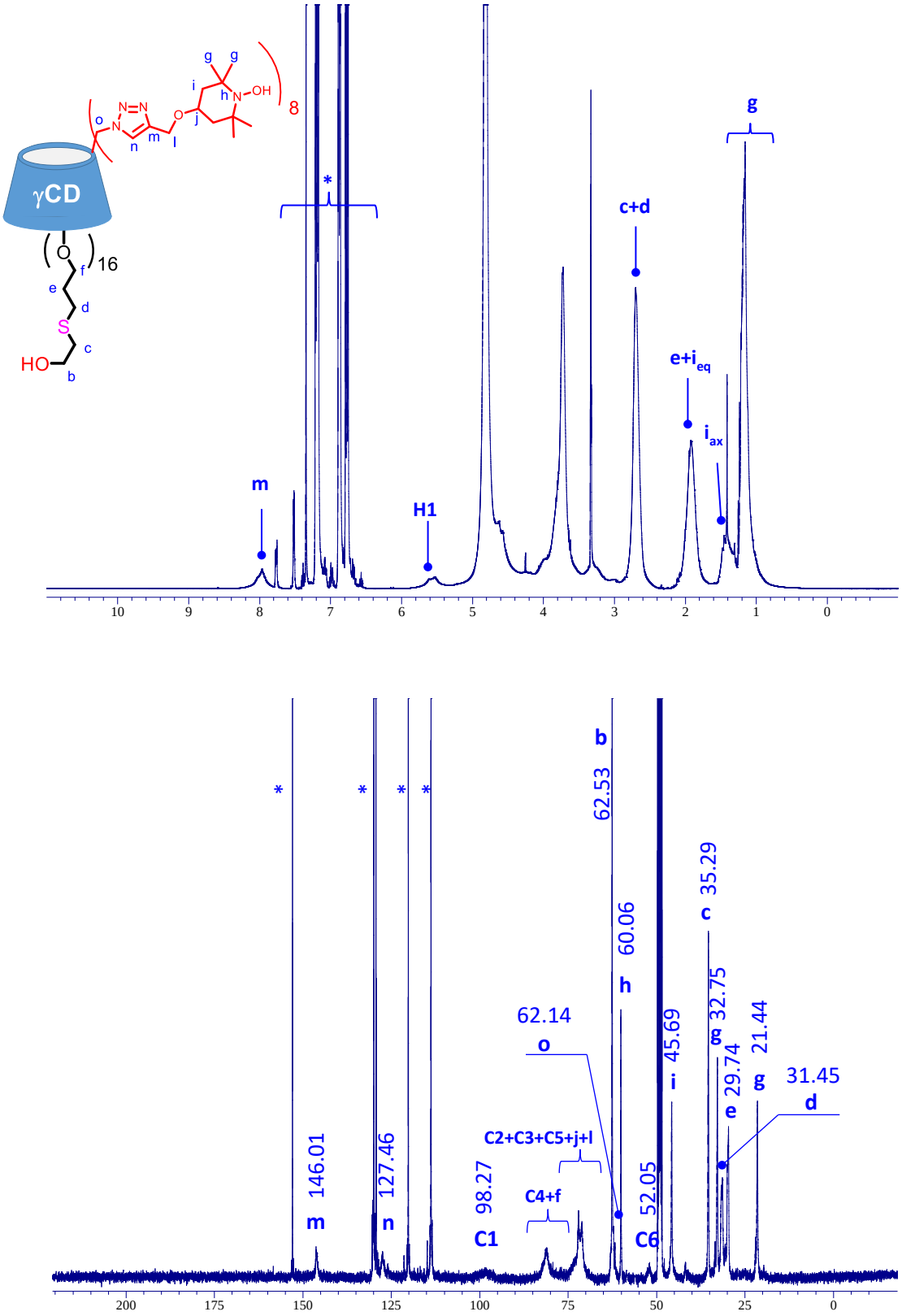

Fig.S16. ^{1}H and ^{13}C NMR spectra of **CD86** after the addition of phenylhydrazine (*). Solvent: methanol-d_3.

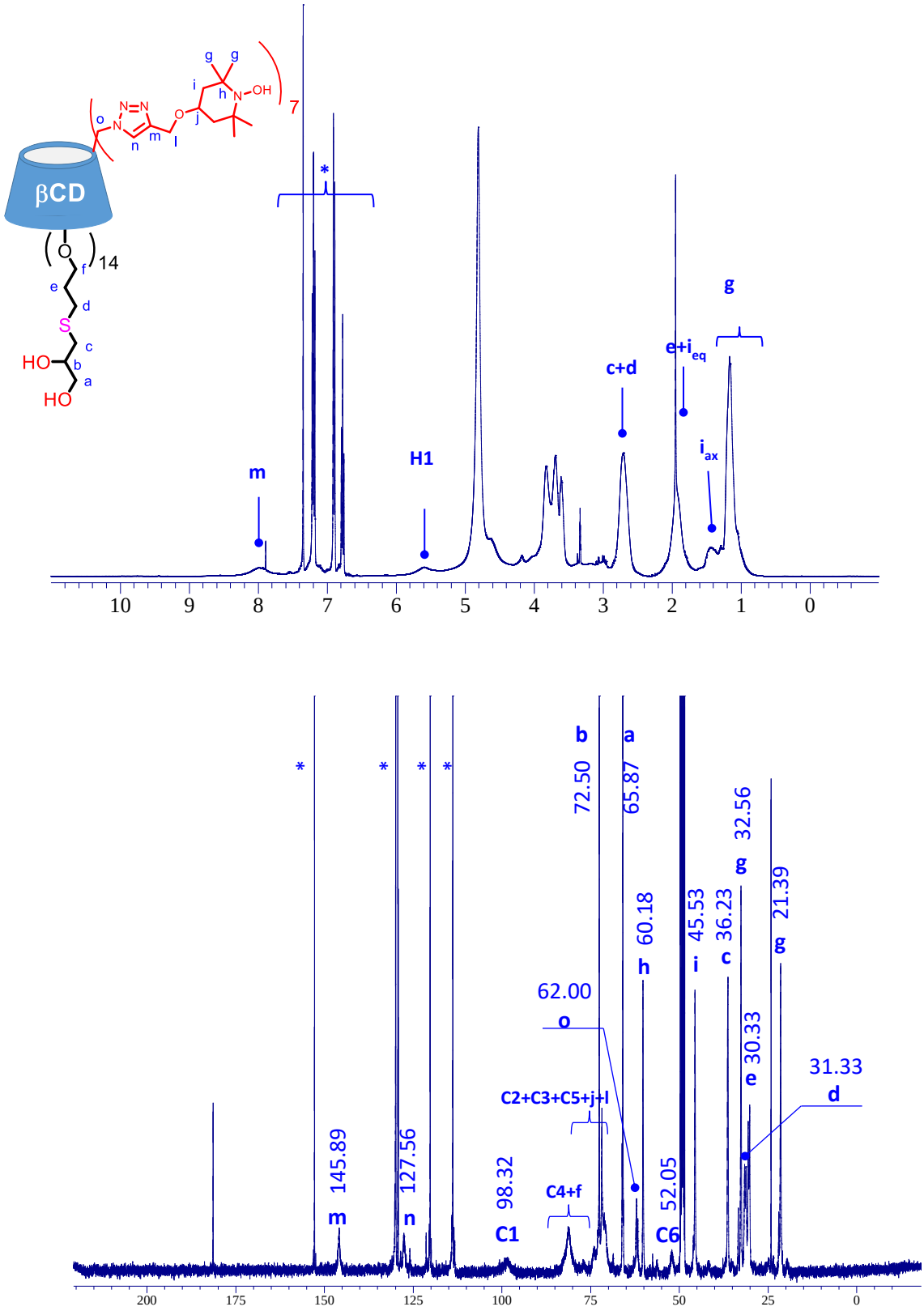

Fig. S17. ^{1}H and ^{13}C NMR spectra of **CD77** after the addition of phenylhydrazine (*). Solvent: methanol-d_3.

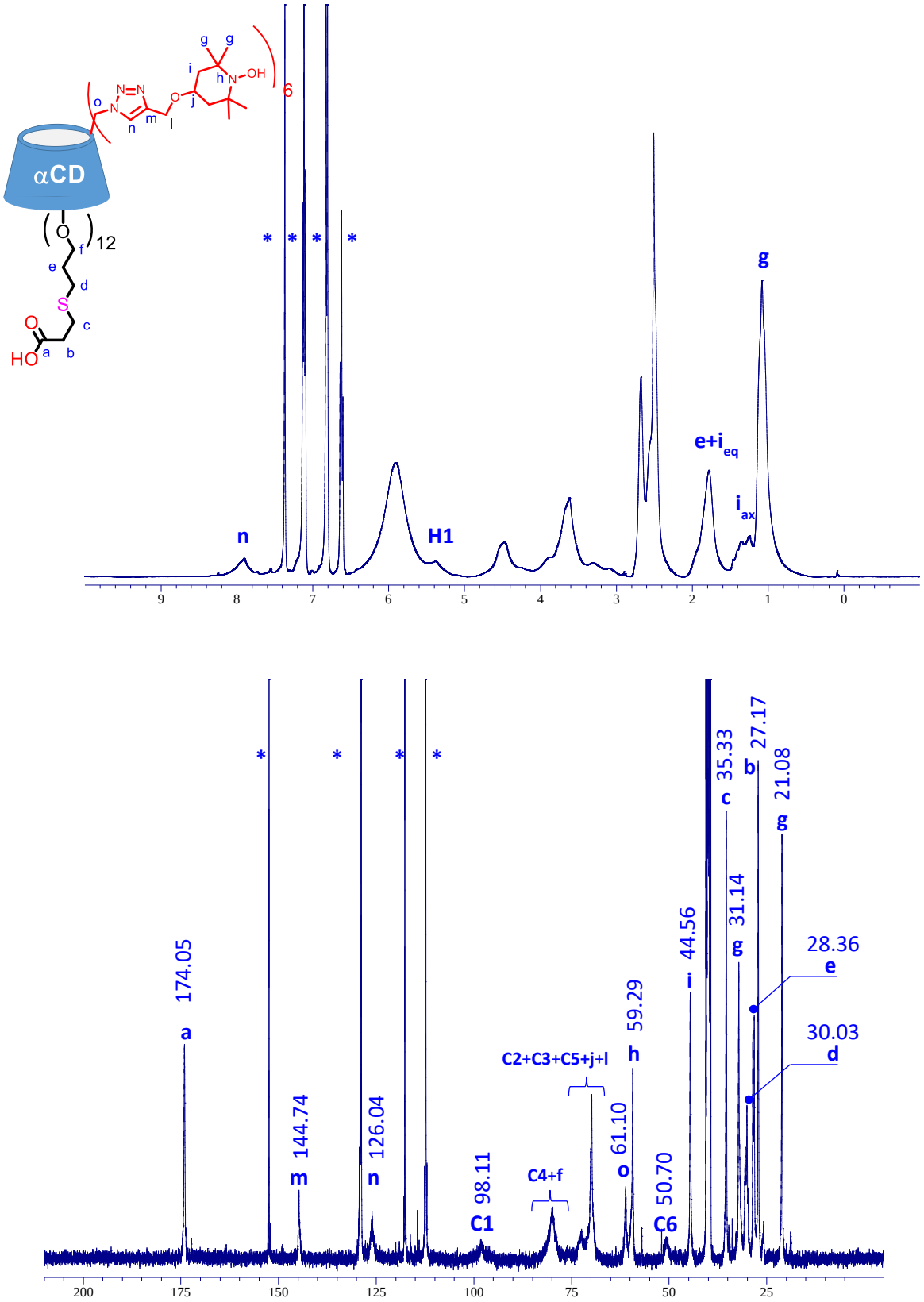

Fig.S18. ^{1}H and ^{13}C NMR spectra of **CD68** (as carboxylic acid) after the addition of phenylhydrazine (*). Solvent: DMSO-d_6.

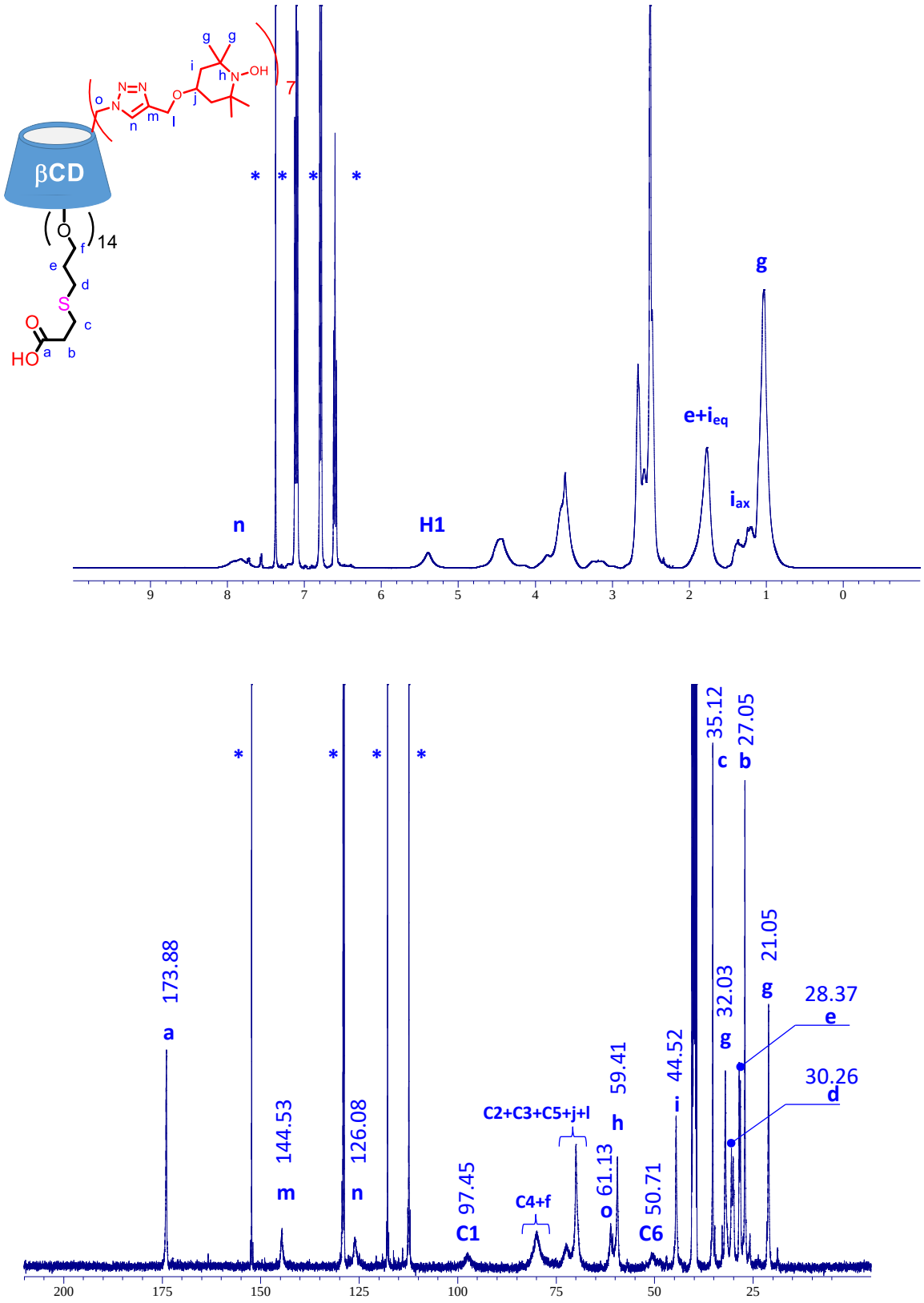

Fig.S19. ^{1}H NMR and ^{13}C NMR spectra of **CD78** (as carboxylic acid) after the addition of phenylhydrazine (*). Solvent: DMSO-d_6.

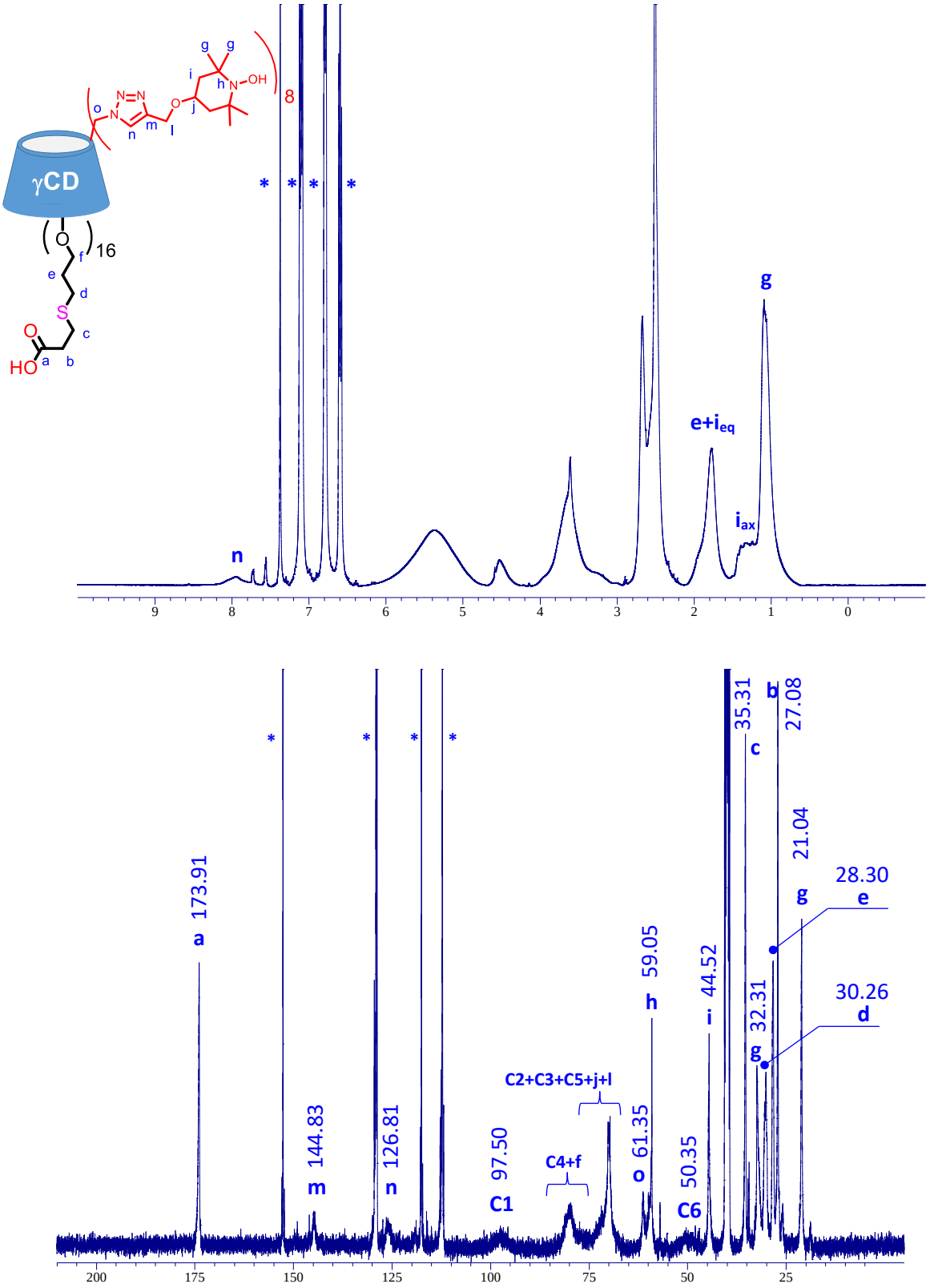

Fig.S20. ^{1}H NMR and ^{13}C NMR spectra of **CD88** (as carboxylic acid) after the addition of phenylhydrazine (*). Solvent: DMSO-d_6.

ESI-MS

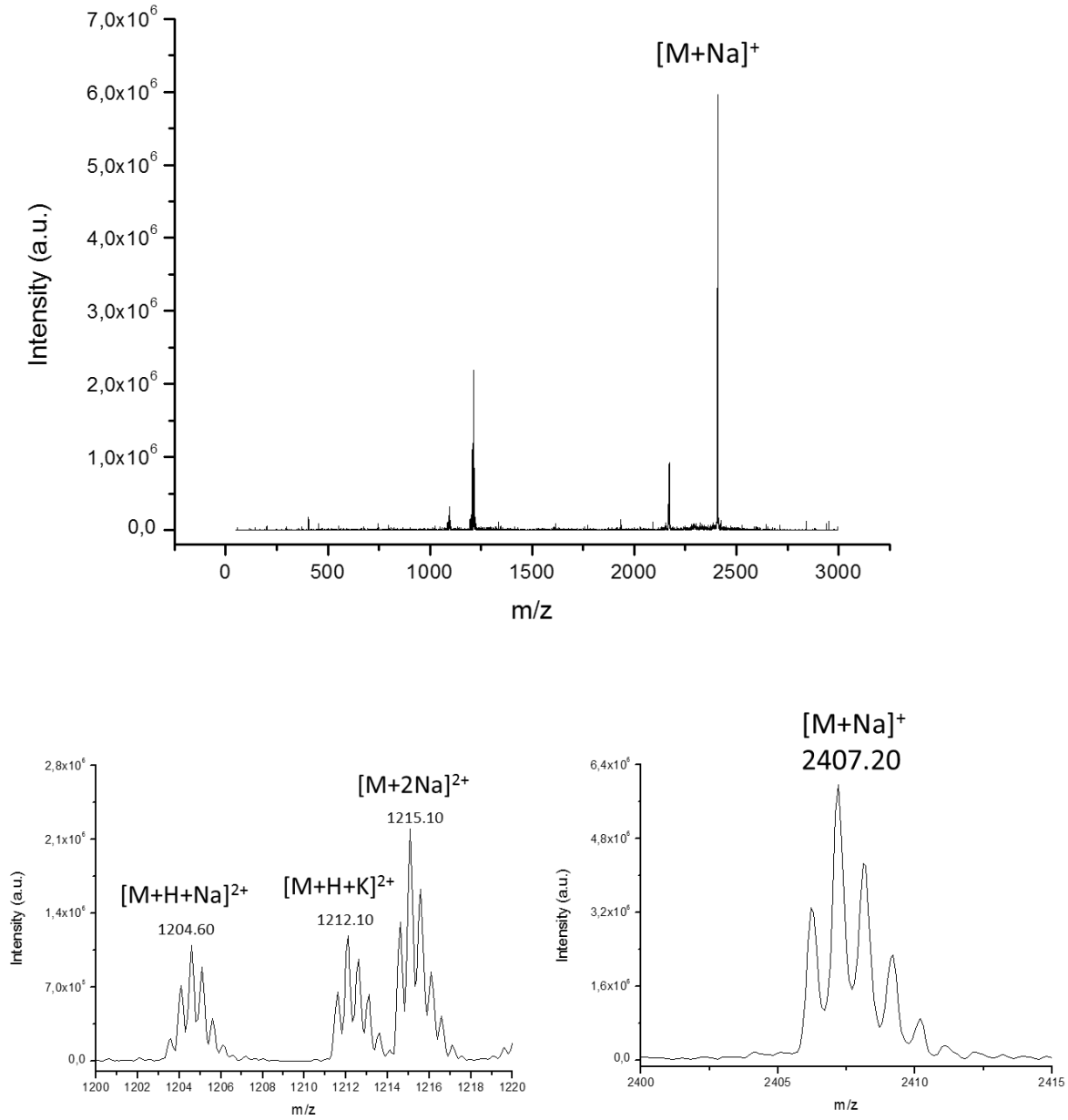

Fig.S25. ESI-MS spectrum (positive) of **CD61**.

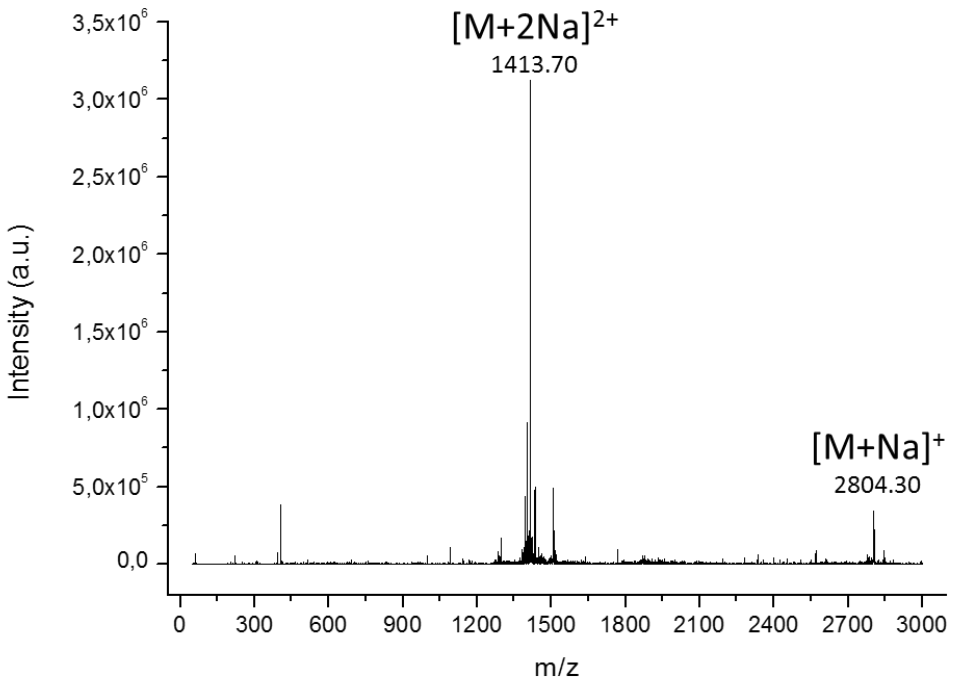

Fig.S26. ESI-MS spectrum (positive) of **CD71**.

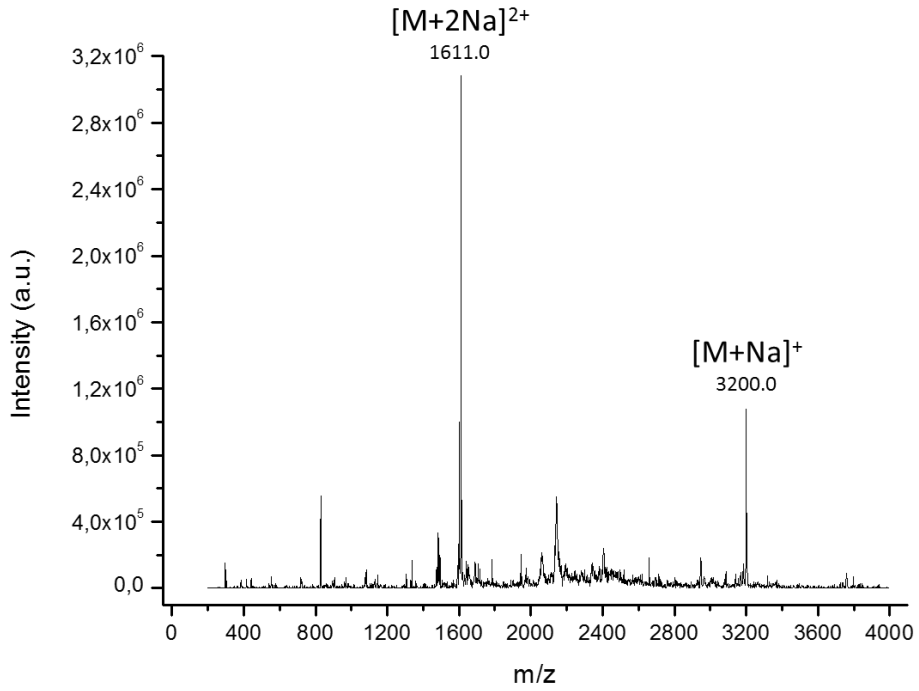

Fig.S27. ESI-MS spectrum (positive) of **CD81**.

T_1 measurements

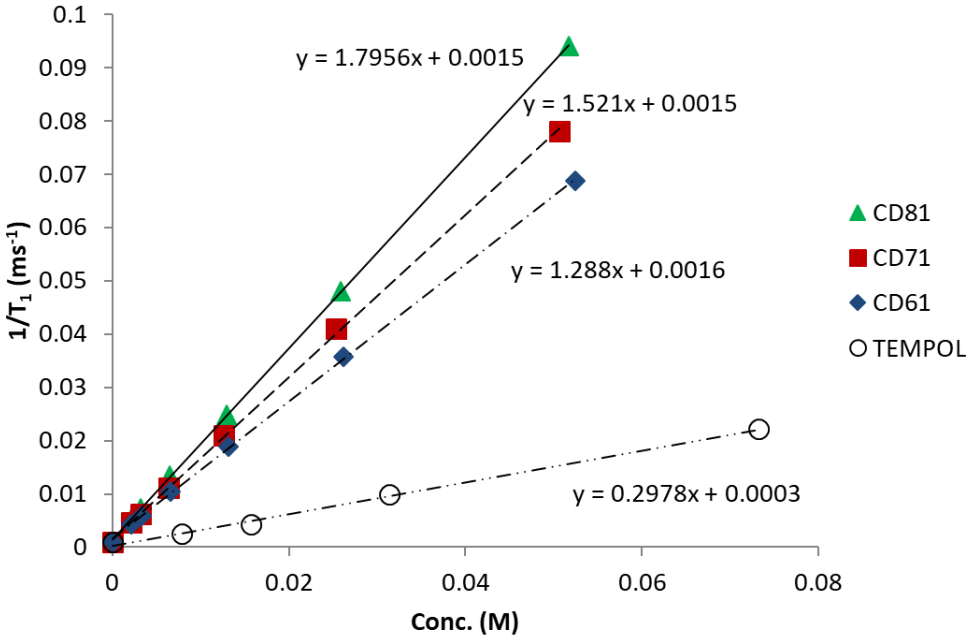

Fig. S28. Relaxivity measurements for **CD61**, **CD71**, **CD8** and TEMPOL. Solvent: DMSO-d_6/H_2O 9:1 (v:v). Temperature: 300 K.

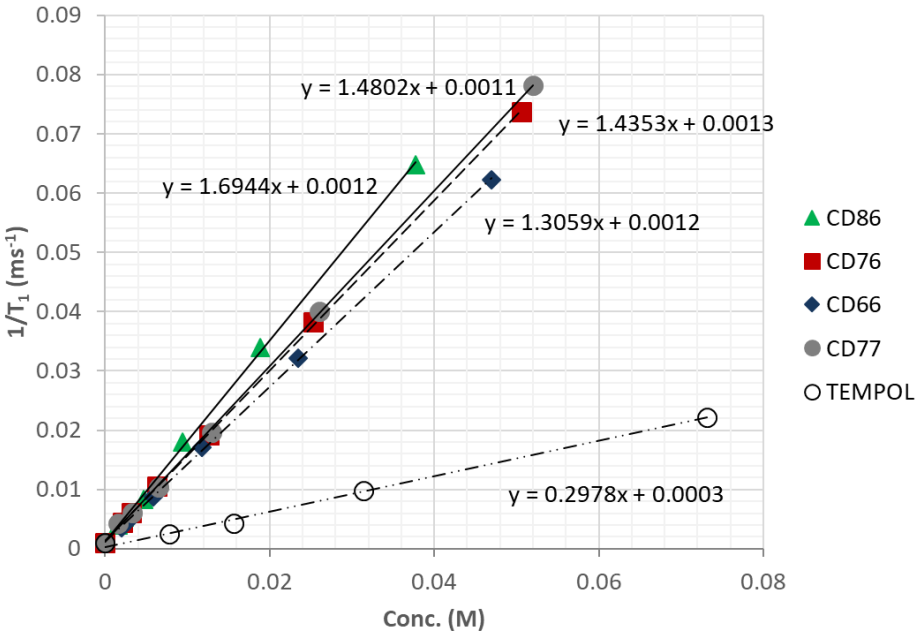

Fig. S29. Relaxivity measurements for **CD66**, **CD76**, **CD86**, **CD77** and TEMPOL. Solvent: DMSO-d_6/H_2O 9:1 (v:v). Temperature: 300 K.

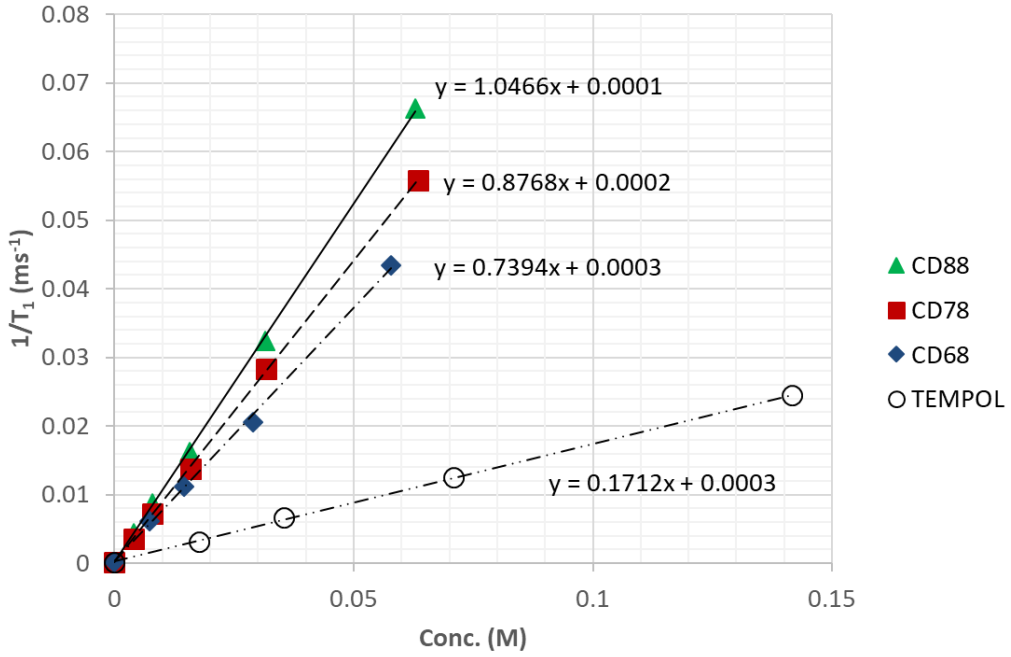

Fig. S30. Relaxivity measurements for **CD68**, **CD78** and **CD88** and TEMPOL. Solvent: D_2O/H_2O 9:1 (v:v). Temperature: 300 K.

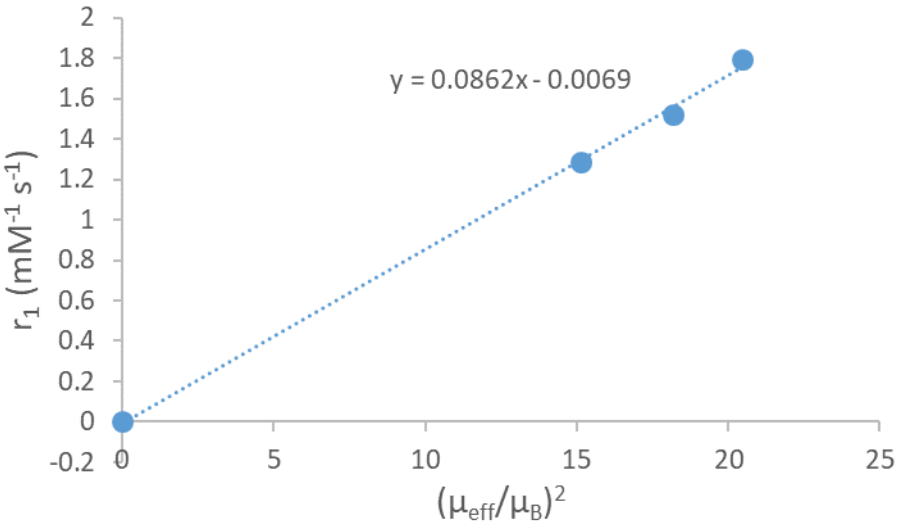

Fig.S31. r_1 vs μ_{eff}^2 for compounds **CDn1**, n=6,7,8.

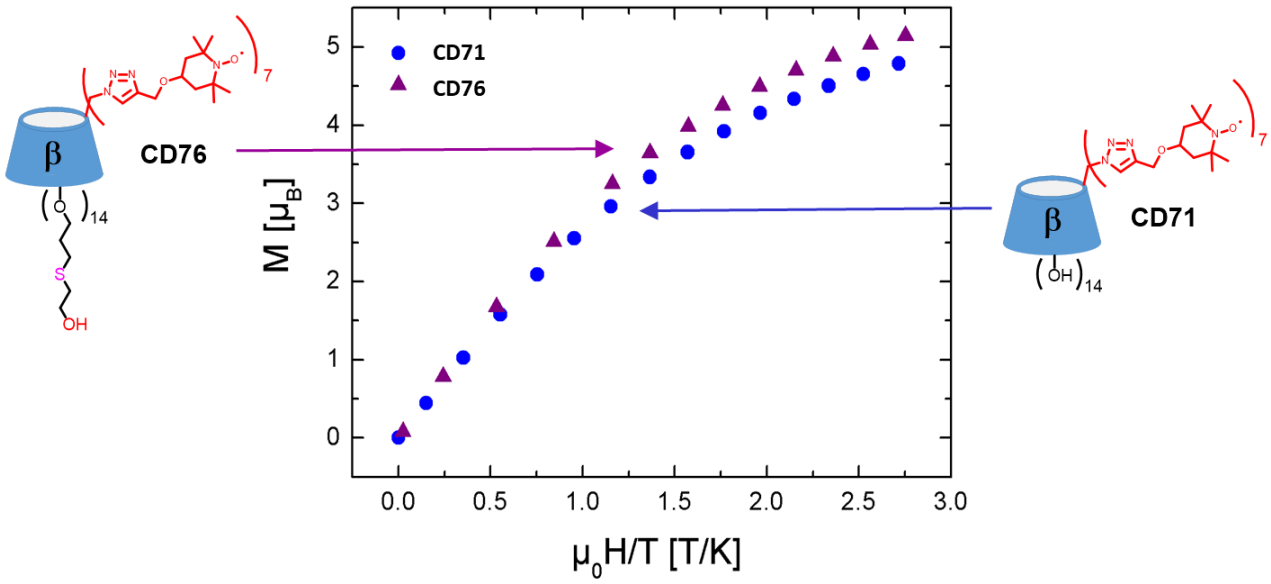

Fig. S32. Isothermal magnetization data of **CD71** and **CD76** as a function of H/T (at T=2 K).

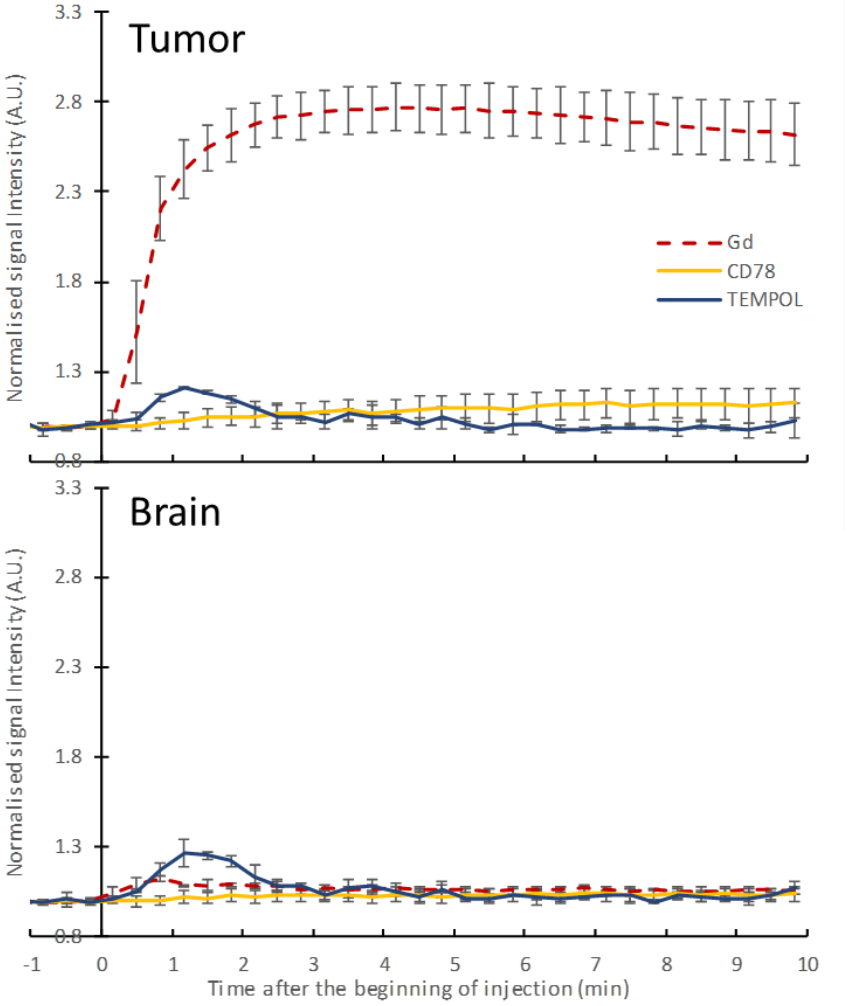

Fig. S33. Change of T_1-weighted in vivo gradient-echo MR signal (repetition time 156 ms, echo time 4 ms, flip angle 90 degrees, measured at 9.4 T) following tail vein injection of contrast agent (either 0.2 mmol/kg of Gd-DTPA or **CD78,** or 1.6 mmol/kg TEMPOL) in tumor (top) and brain (bottom)tissue. Markedly different kinetics were observed for different contrast agents. TEMPOL showed a similar transient contrast increase for both tumor and brain tissue, whereas both Gd-DTPA and **CD78** showed larger change in tumor tissue. **CD78** accumulated to tumor tissue more slowly than Gd-DTPA.

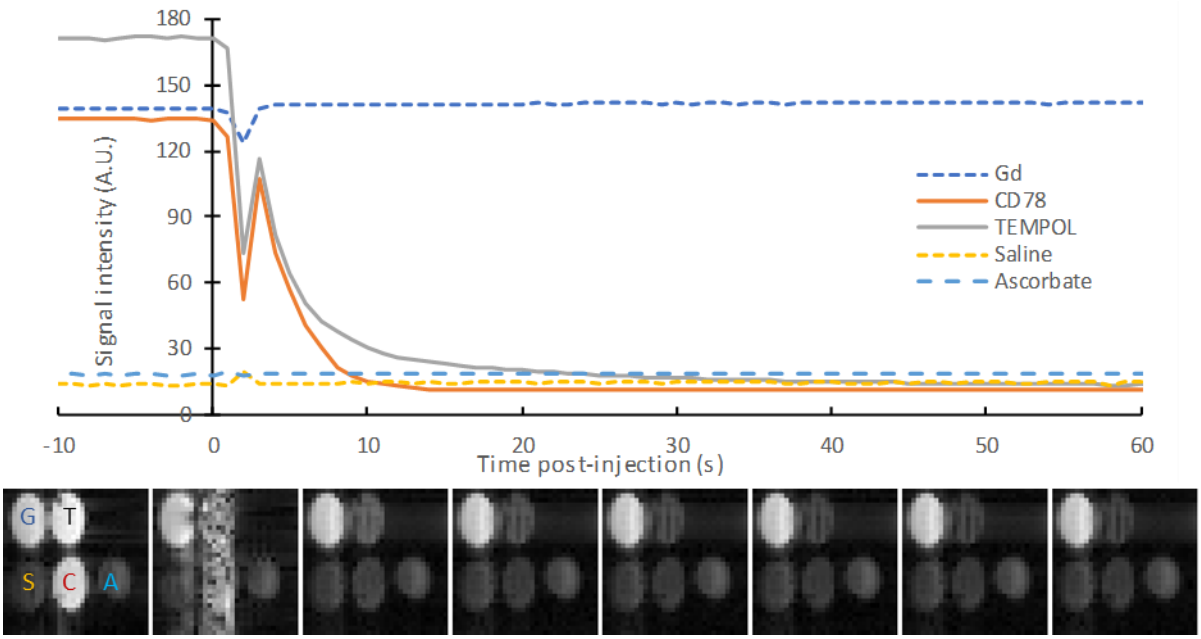

Fig. S34. Change of T_1-weighted gradient-echo MR signal (repetition time 31 ms, echo time 1.1 ms, flip angle 60 degrees, field of view 40x24 mm, data matrix 32x32, slice thickness 2 mm, measured at 9.4 T) during the addition of sodium of ascorbate (200 µl of 2.6 M, final concentration in sample 525 mM, 3-fold excess to the amount of TEMPOL moieties) to **CD78** (in 800 µl saline, final concentration 25 mM) and TEMPOL (in 800 µl saline, final concentration 175 mM) samples. For reference, signals from saline, 2.6 M ascorbate and Gd-contrast agent (5 mM Clariscan) are also shown. A rapid of loss signal, indicating reduction of TEMPOL, was observed in both **CD78** and TEMPOL samples after addition of ascorbate. Corresponding T_1 values are reported in Table S1.

Table S1. In vitro T_1 relaxation times (s) before and after addition of sodium ascorbate

	GD	CD78	TEMPOL	SALINE	ASCORBATE
PRE-INJECTION	31 ms	20 ms	17 ms	2.8 s	1.4 s
POST-INJECTION	26 ms	2.0 s	2.4 s	2.8 s	1.4 s